Molecular Simulation of Transport in Liquids and Polymers

Vom Fachbereich Chemie
der Technischen Universität Darmstadt

zur Erlangung des akademischen Grades
eines Doktor rerum naturalium (Dr. rer. nat.)

genehmigte
Dissertation

vorgelegt von

Eduard Rossinsky, M.Sc. of Chemical Engineering

Aus Belgorod, Russian Federation

Berichterstatter:	Prof. Dr. Florian Müller-Plathe
Mitberichterstatter:	Prof. Dr. Rolf Schäfer
Eingereicht am:	01.12.2009
Mündliche Prüfung am:	18.01.2010

Darmstadt 2010
D17

Acknowledgements

First of all, I would like to gratefully acknowledge the enthusiastic supervision of Prof. Dr. Florian Müller-Plathe during this work. I am very grateful to him for giving me the opportunity to work in his group. I will always be thankful for his wisdom, knowledge, and deep concern. He has always been supportive and has given me the freedom to pursue various projects without objection. He has also provided many relevant and insightful discussions during this research. It has been a real honour to work with him.

I would like to thank all my colleagues for creating a warm working-atmosphere. Particularly, I would like to say a special thank-you to Konstantin B. Tarmyshov for his help in facilitating my adjustment to the life in Darmstadt, and for his scientific support. I am grateful to Michael C. Börn and Pavel Polyakov for their helpful discussions and for their help during the final stages of this thesis. A special thanks to Gabriele General for her positive outlook and her ability to smile in spite of any difficulties.

I would like to convey my heartfelt thanks to my home university, the Technion, which helped me to achieve this high level of education. And of course, in the end, I would like to mention, with special thanks, the support I received from my family and my friends in Germany and Israel.

Table of Contents

List of Figures

List of Tables

Abstract

Computer simulations of complex multi- particle systems have attracted more and more research interest. Molecular dynamics (MD) simulations have been used intensively in various scientific fields such as molecular biology, polymer physics, nanotechnology and many others. System properties measured at a certain time can be deduced from the coordinates and velocities of classical particles. If the interatomic forces are known with a good accuracy and the initial conditions of the system can be defined properly, molecular dynamics simulation can act as a computer simulation. It means that these results can be compared to experimentally obtained values and, more importantly, some other information about the system can be accessed, which sometimes is hard or impossible to measure. After a short overview on MD methods, several MD simulations will be presented.

Thermal conductivity of polymer crystals is a typical quantity that is difficult to experimentally determine. This is because samples of large-enough single crystals of polymers for thermal conductivity measurements have not yet been prepared, therefore the single crystal properties can only be determined via computer simulation. In Chapter 3 we have summarized extensive calculations of the thermal conductivity of the δ-phase of syndiotactic polystyrene (sPS). Until now, only partial theoretical data dealing with thermal conductivity of crystalline polymers was available.

This available data was particularly concerned with the correlation between thermal conductivity and the polymer's morphology and orientation [D. Hansen and G. A. Bernier, Polym. Eng. Sci. **12** (3), 204 (1972)]. In comparison with the amorphous structure of polymer a large anisotropy can be established in crystalline polymer as result of varied structural and morphological parameters in different directions. MD simulations permit us, for example, to restrict some oscillations and to set the bond length between two atoms, which can be done by addition of constraints in the system. Such artificial constraints limit the free movement of the particles which decreases the degrees of freedom of the system. In this study we investigated the sensitivity of the thermal conductivity to different numbers and locations of such constraints in different parts of

the polymeric chains. It was found that the thermal conductivity has a tendency to decrease when the number of active degrees of freedom in the system is reduced by the introduction of stiff bonds. This dependence is, however, weaker and more erratic than previously found for molecular liquids and amorphous polymers [E. Lussetti, T. Terao, and F. Müller-Plathe, J, of Phys, Chem, B **111** (39), 11516 (2007)].

Another physical property of polymers, which has attracted a great deal of attention from researchers in the recent times, is the understanding of the dynamic and static properties of polymer chains. Many technologies such as electronics packaging, coatings, adhesion, and composite materials are based on these polymeric properties. In Chapter 4 we discussed the physical properties of short polyvinyl-alcohol (PVA) oligomers up to a chain length of ten monomers chain ($H(-CH_2-CH(OH)-)_NCH_3$). The specific volume was found to depend linearly on the inverse number of repeat units N, a result that is in agreement with experimental findings for other polymers. The gyration radius was found to depend on the number of formula units via $N^{0.65\pm0.03}$. The exponent simulated is somewhat larger than the known $N^{0.588}$ dependence for long chains in good solvents. We also discuss the orientation correlation function for different bonds in the chain. The relaxation times for these bond vectors, as obtained via the Kohlrausch-Williams-Watt expression, showed an exponential dependence on the number of repeat units.

In Chapter 3 we studied the thermal conductivity of crystal polymer but under certain conditions and as a response to a temperature gradient, it was possible to correlate the separation between different chemical species. This effect is called the Soret effect or thermal diffusion effect and is quantified by the Soret coefficient (S_T). Although this effect has been studied for more than 150 years, a microscopic understanding of thermal diffusion processes in liquids is still unavailable. The precise prediction of S_T from theory and simulations and even the experimental determination for more complex systems is often a challenge. In Chapter 5, we studied the thermal diffusion behavior of an equimolar mixture of hydrocarbon chains in xylene. Hydrocarbon chains (alkanes and alkenes) with the same carbon number were considered in order to exclude the mass

contribution and to investigate the influence of molecular structure on the Soret coefficient. Thermal diffusion behavior was analyzed in terms of static and dynamic properties of the mixtures and an explanation for the observed results has been supplied.

Chapter 6 finally summarizes the main conclusions of the present study in the thesis and provides summary of the work.

Zusammenfassung

Computersimulationen komplexer Vierteilchen-Systeme haben in den letzten Jahren an Bedeutung gewonnen. Besonders Simulationen vom Molekular-Dynamik (MD)-Typ wurden vielfach benutzt, um Probleme aus dem Bereich der Molekularbiologie, der Polymer-Physik, der Nanotechnologie und ähnlicher Felder zu behandeln. Innerhalb bestimmter Zeitskalen können die Eigenschaften von Systemen auf Basis der Koordinaten und Geschwindigkeiten von klassischen Teilchen mit MD berechnet werden. Mithilfe genügend genauer Wechselwirkungspotentiale und definierten Anfangsbedingungen ist es möglich, Molekular-Dynamik-Simulationen durchzuführen. Die Ergebnisse dieser Rechnungen können mit experimentellen Daten verglichen werden. In Fällen, in denen experimentelle Ergebnisse nicht zugänglich sind, liefern die Computersimulationen den einzigen Zugang zu Systemeigenschaften. Nach einem kurzen Überblick über MD-Methoden, möchte ich in dieser Arbeit einige MD-Simulationen vorstellen.

Die thermische Leitfähigkeit von Polymerkristallen ist zum Beispiel eine Eigenschaft, die experimentell schwierig zu bestimmen ist. Dies liegt daran, dass genügend große Einkristalle von Polymeren noch nicht präpariert werden konnten. Das Verhalten solcher Einkristalle lässt sich deshalb nur am Computer bestimmen. Solche Simulationen möchte ich in Kapitel 3 für die thermische Leitfähigkeit der δ-Phase des syndiotaktischen Polystyrols (PS) beschreiben. Bis jetzt sind nur wenig theoretische Ergebnisse zur thermischen Leitfähigkeit kristalliner Polymere publiziert worden.

Die wenigen zugänglichen Daten haben sich mit der Korrelation zwischen thermischer Leitfähigkeit und der Morphologie bzw. Orientierung von Polymeren beschäftigt [D. Hansen and G. A. Bernier, Polym. Eng. Sci. **12** (3), 204 (1972)]. Im Unterschied zu amorphen Polymeren können kristalline Polymere aufgrund morphologischer und struktureller Parameter gewisse Anisotropen aufweisen. MD-Simulationen an solchen Systemen können unter bestimmten Einschränkungen durchgeführt werden, z.B. dem Festhalten von Bindungen. Diese künstlichen Beschränkungen limitieren die Bewegung der Teilchen.

In der vorliegenden Arbeit habe ich die Veränderung der thermischen Leitfähigkeit als Funktion der Anzahl und Position festgehaltener Freiheitsgrade in einem

Polymer untersucht. Wie erwartet, stellte sich heraus, dass die thermische Leitfähigkeit kleiner wird, wenn Freiheitsgrade im System durch die Einführung steifer Bindungen eingefroren werden. Diese Abhängigkeit ist in der von mir untersuchten δ-Phase von Polystyrol aber kleiner als in molekularen Flüssigkeiten und amorphen Polymeren [E. Lussetti, T. Terao, and F. Müller-Plathe, J, of Phys, Chem, B **111** (39), 11516 (2007)].

Viele Wissenschaftler haben sich in den letzten Jahren dem Verständnis dynamischer und statischer Eigenschaften von Polymerketten gewidmet. Für viele Technologien im Bereich der Halbleiter, Lacke, Adhäsion und Komposit-Materialien sind diese Eigenschaften wichtig. In Kapital 4 möchte ich die physikalischen Eigenschaften von Polyvinyl-Alkohol (PVA)-Oligomeren mit Kettenlängen bis zu 10 Monomeren ($H(-CH_2-CH(OH)-)_NCH_3$) vorstellen. Ich konnte zeigen, dass das spezifische Volumen linear von der reziproken Anzahl N der Monomereinheiten abhängt. Diese Abhängigkeit wurde experimentell bei anderen Polymersystemen bestätigt. Für den Trägheitsradius R_g wurde eine $N^{0.65\pm0.03}$ Abhängigkeit gefunden. Der in dieser Arbeit ermittelte Exponent ist etwas größer als die bekannte $N^{0.588}$-Abhängigkeit für lange Ketten in guten Lösungsmitteln. In Kapitel 4 diskutiere ich ebenfalls die Orientierungs-Korrelationsfunktion verschiedener Bindungen in der Kette. Die Relaxationszeiten dieser Bindungsvektoren wurden im Rahmen der Kohlrausch-Williams-Watts-Theorie berechnet. Sie zeigen die erwartete exponentielle Abhängigkeit als Funktion der Anzahl der monomeren Baueinheiten.

In Kapitel 3 beschäftige ich mich mit der thermischen Leitfähigkeit eines kristallinen Polymers unter verschiedenen Randbedingungen. Durch die „Antwort“ auf einen Temperatur-Gradienten war es möglich, die Entfernung zwischen den verschiedenen chemischen Komponenten zu bestimmen. Dieser Effekt, i.e. Thermodiffusion, wird durch den sogenannten Soret-Koeffizienten (S_T) beschrieben. Obwohl dieses Phänomen schon seit 150 Jahren bekannt ist, existiert bis heute kein mikroskopisches Bild für die Thermodiffusion in Flüssigkeiten. Eine halbwegs genaue Bestimmung von S_T entweder durch Simulationen oder experimentell stellt für komplexe Systeme immer noch eine Herausforderung dar. In Kapitel 5 beschreibe ich die thermische Diffusion in einer äquimolaren Mischung reiner Kohlenwasserstoffe in Xylol. Dabei wurden Alkan- und Alken-Ketten mit der gleichen Anzahl von Kohlenstoff-

Atomen verwendet, um Masseneinflüsse auf S_T auszuschließen und nur den strukturellen Einfluss auf den Soret-Koeffizienten zu bestimmen. Die thermische Diffusion in diesem System wurde mithilfe statischer und dynamischer Eigenschaften analysiert und erklärt.

In Kapitel 6 fasse ich noch einmal die wichtigsten Ergebnisse der vorliegenden Doktorarbeit zusammen.

Chapter 1: Introduction

The availability of modern, high speed computers rendered possible the intensive application of computational methods for scientific investigations. Although limited to approximate simulations of simple model systems in the early days, computational techniques are now capable of accurately modeling and investigating relevant, complex systems, such as polymers in different environments. The work presented in this thesis involves the application of computational methods to several areas. One of the topics studied was the thermal conductivity of polymer crystal. For this research the δ phase of syndiotactic polystyrene has been chosen. Another application of computational methods for the study of molecular dynamics is the investigation of the physical properties of poly-vinyl-alcohol oligomers. The third topic studied and reported in this dissertation deals with computation of the Soret coefficient in equimolar mixtures of xylene/alkanes(enes).

The first steps in the study of these subjects were taken in the beginning of the 1960's as part of fundamental research in the statistical mechanics of macromolecules[1]. For research in this area Stanford University Professor, Paul J. Flory, was awarded the Nobel Price in 1974. At the present time, we have to note the research of the French physicist Pierre-Gilles de Gennes who described the dynamic properties of polymers. In his famous monograph, he mentioned several main points for progress in polymer science and one of them was the advancement in computer simulation. The methods of computer simulations that have been applied in this thesis is molecular dynamics (MD) and will be described in detail in Section 2.

The significance of synthetic polymers and the role of natural macromolecules like proteins, polysaccharides, and nucleic acids in biological systems are well known. In spite of extremely wide variations in the chemical structure of macromolecules, it is possible to identify a few typical characteristics of polymers. One of these is their ability to change structure as a function of temperature and environment. Another characteristic that is unique to polymers is the low entropy of the system, which can be explained by

the covalent bonding of the atoms forming the backbone, so that they cannot move without shifting their neighbors. Therefore the physical properties of oriented polymers are exceptional, as will be illustrated in Chapter 3, with respect to thermal conductivity behavior.

In this chapter we calculated the thermal conductivity of crystalline polystyrene. Polystyrene, abbreviated as PS, is witnessing increasing interest nowadays due to its various technical applications. This polymer is becoming more and more common in the production of electrical and electronic devises because of its electrical properties[2]. But, in order to estimate heat dissipation in electrical devices it is necessary to know the value of the thermal conductivity of the material at room temperature range. Additionally, appreciable levels of thermal conductance are needed for use of polystyrene in circuit boards, heat exchangers, and machinery[3]. Due to the tendency of polystyrene to be in crystal form of its enantiomers (isotactic and syndiotactic polymers) it is also important to know about the crystallinity of PS along with its thermal conductivity. However, until a pure crystal is obtained, the thermal conductivity of the crystalline polymer can be estimated only by simulation.

Data on thermal conductivity has been reported for many polymers, but surprisingly little has been said about the relationship of thermal conductivity to such parameters as crystallinity and molecular orientation. The data of Hennig and Knappe[4] shows for a uniaxially-oriented polymers that the thermal conductivity increases in the direction of chain orientation ($\lambda_{\parallel}$) with a corresponding decrease in directions normal to the orientation ($\lambda_{\perp}$). However, the difference between those two values depends on the morphology of the polymer. For example, in the crystal form of quartz crystals $\lambda_{\parallel}/\lambda_{\perp}$=1.7, while in a simple polymer as polyethylene $\lambda_{\parallel}/\lambda_{\perp} \approx 100$.[5] In our work, this value has been estimated for crystal polystyrene δ phase and for its collapse structure with density close to α/β forms of crystal structure.

Chapter 4 describes the physical properties of another polymer, polyvinyl alcohol (PVA) oligomers. The physical property has been studied as for polystyrene, and in this case, concerning its use in industry, the thermal conductivity is less crucial. PVA is a

synthetic polymer used since the early 1930s in a wide range of industrial, medical and food applications. In textiles for example, the polymer is applied as a sizing and coating agent. It provides stiffness to certain products making them useful for tube winding, carton sealing and board lamination. PVA is also used as a thickening agent for latex paint and common household white glue or in other adhesive mixtures.[6] This wide application of the polymer demands careful studies of the polymer bulk. In our MD simulation we calculated the physical PVA oligomer's properties which are usually used for discrimination between bulk and interface: radius of gyration, radial distribution function between different kinds of atoms in the molecule and the orientation correlation function of some bonds. Some of our results have been compared to experimental data and theoretical studies, and for both comparisons good agreement has been found[7]. Therefore this simulation can serve as reference data for future work on interfaces.

The same method which has been implied for the calculation of thermal conductivity of crystal polymer (Chapter 3) can be used for studies of an equally important property called the Soret effect. Thermodiffusion, also called thermal diffusion or the Ludwig–Soret effect, describes the partial separation of mixture components when the system is set in thermal gradients. Although Ludwig and Soret discovered the effect almost two hundred years ago, to date there is no full molecular understanding of the thermodiffusion in liquids. This effect plays an important role in many naturally occurring processes such as the, component segregation in solidifying metallic alloys or volcanic lava[8] and and perhaps convection in stars_[9]. Technical applications for the process exempli gratia are isotope separations of liquids and gaseous mixtures, the thermal field flow fractionation of polymers[10], the identification and separation of crude oil components[11], the coating of metallic items, etc. On the basis of theoretical models, simulations, and recent experiments we elucidated some properties and mechanisms contributing to the Soret effect. For example, we know that the Soret effect is affected by the mass and size of particles, the interaction potential, and the composition of the mixture[12]. In our simulations, we chose components of the same mass, size and

interactions. Therefore we could study the effect of the structure on the Soret effect which is shown in Chapter 5.

References

[1] P. J. Flory, Butterworth-Heinemann Ltd (1969).

[2] I. Krupa, I. Novak, and I. Chodak, Synth. Met. **145** (2-3), 245 (2004).

[3] Y. He, B. E. Moreira, A. Overson, S. H. Nakamura, C. Bider, and J. F. Briscoe, Thermochim. Acta **357**, 1 (2000).

[4] K. H. Hellwege, W. Knappe, and J. Hennig, Acta. Vet. Acad. Sci. Hungar. **13** (4), 121 (1963); J. Hennig and W. Knappe, J. Pol. Sci. Part C-Polymer Symposium (6PC), 167 (1964).

[5] D. B. Mergenthaler and M. Pietralla, Z. Phys. B-Condens. Mat. **94** (4), 461 (1994).

[6] C. M. Hassan and N. A. Peppas, in *Biopolymers/Pva Hydrogels/Anionic Polymerisation Nanocomposites* (SPRINGER-VERLAG BERLIN, Berlin, 2000), Vol. 153, pp. 37.

[7] R. L. Davidson, *Handbook of water-soluble gums and resins*. (MacGraw-Hill, New York, 1980); J. des Cloiseaux and G. Jannink, Polymer in Solution; Their Modelling and Structure **Clarendon, Oxford** (1990); W. Dollhopf, H. P. Grossmann, and U. Leute, Colloid Polym. Sci. **259** (2), 267 (1981).

[8] R. T. Cygan and C. R. Carrigan, Chem. Geol. **95** (3-4), 201 (1992).

[9] E. A. Spiegel, Annu. Rev. Astron. Astrophys. **10**, 261 (1972).

[10] M. E. Schimpf and J. C. Giddings, J. Pol. Sci. Part B-Polymer Phys. **27** (6), 1317 (1989).

[11] P. Costeseque, D. Fargue, and P. Jamet, Thermal Nonequilibrium Phenomena in Fluid Mixture **584**, 389 (2002).

[12] P. Bordat, D. Reith, and F. Müller-Plathe, J. Chem. Phys. **115** (19), 8978 (2001); D. Reith and F. Müller-Plathe, J. Chem. Phys. **112** (5), 2436 (2000).

Chapter 2: Theory and method

2.1 *Thermal conductivity*

Heat is a form of energy that is transferred between two boundaries of a system based on a temperature difference, the transfer being from the boundary at the higher temperature to the boundary at the lower one. It is a transient phenomenon. Fourier's law of conduction gives the relationship between heat flow and the temperature gradient for a homogeneous, isotropic solid in steady state. It is important to note, that the method which has been used for the thermal conductivity calculation, and which will be described later, is based on this law. It can be written in the form of:

$J(\vec{r},t) = -\lambda \nabla T(\vec{r},t)$

where $J(\vec{r},t)$ is the heat flux vector in the opposite direction of the temperature gradient, $\nabla T(\vec{r},t)$ is the temperature gradient vector, and the constant of proportionality, λ , is the thermal conductivity of the material. It is a positive, scalar quantity. The minus sign is to make the heat flow a positive quantity, since the direction of heat flow is toward decreasing temperature.

Thermal conductivity, λ, is a physical property of the conducting material. Sometimes, it is called a transport property because for a given temperature gradient, heat flux is directly proportional to thermal conductivity. Thus, thermal conductivity is an important property in thermal analysis.

2.2 *Soret effect*

2.2.1 Theory and calculation

The Soret effect or the so called thermal diffusion is the tendency of a mixture of two or more components to separate as a result of a spatial temperature difference. The theory is based on the assumption that in steady state the component concentration and temperature profile between the hot and the cold region are linear functions and then the Soret effect is quantified by the equation:

$$S_T = -\frac{1}{x_i(1-x_i)}\frac{dx_i}{dT}$$

where x_i is the mole fraction of component *i, dT is* the temperature gradient and dx_i is the concentration gradient. According to previous research of our group,[1] for binary mixtures of Lennard-Jones particles, the species with a larger molecular weight tend to move from regions of high temperature to those of lower temperature. Also, for mixtures of similar molecular weight species, the molecules with a larger diameter (σ) tend to diffuse from high temperature to low temperature. And, in spite of a numerous number of publications in the area of thermal diffusion in liquids, solids, polymers, etc., it is still the subject of research.

2.2.2 Thermal Diffusion Forced Rayleigh Scattering

Thermal diffusion Rayleigh scattering technique (TDFRS) is a powerful method which is used to study the Soret effect in liquid mixtures.[2]. The advantages of the method are a small temperature difference (20 mK) and a small fringe spacing (20 mm) which keeps the system close to the thermal equilibrium and allow to avoid the convection problems. In the benchmark test it was demonstrated that TDFRS gives reliable results for organic mixtures as well as for simple aqueous systems, which compare well with other experimental techniques.[3]

Figure 2.1 shows the experimental setup. The beam (an argon-ion laser (488 nm)) is split into two (writing) beams with equal intensity by a beam splitter. The writing beams create an intensity grating in the sample. A built-in mirror based on a piezoelectric ceramic has the role of phase stabilization and phase modulation of the grating. To shift the grating by 180^0, the Pockels cell and the half wave plate were used. A small amount of dye in the sample converts the intensity grating into a temperature grating, which in turn causes a concentration grating by the effect of thermal diffusion. Both gratings contribute to a combined refractive index. The diffraction efficiency of the refractive index grating in the sample cell is monitored by a He-Ne laser with a wavelength

$\lambda = 632.8\ nm$ at the Bragg angle. The diffracted beam and stray light were separated by a filter in front of the detector.

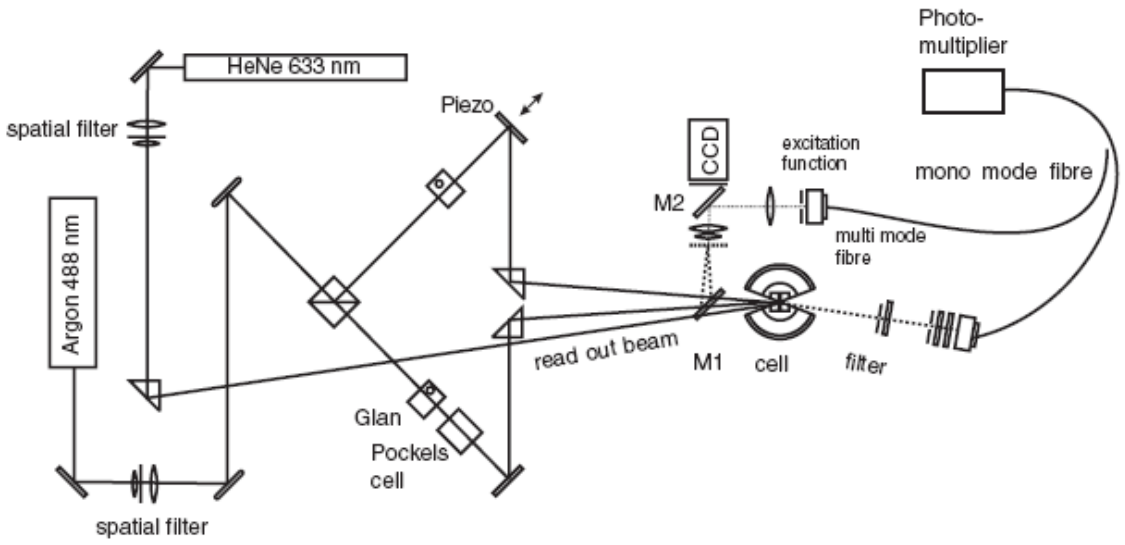

Figure 2.1: Schematic drawing of a thermal diffusion forced Rayleigh scattering (TDFRS) setup. The picture has been taken from previous publication. [4]

The sample cell was installed inside a brass holder and can be adjusted in directions orthogonal to the optical axis. The thickness of the quartz cell (Hellma), which is used for TDFRS measurements, is 0.2 mm. A thermostat (Lauda ubrat) mounted in the brass holder controls the temperature of the sample by a circulating water bath with an uncertainty of $0.2^0 C$. (c.f. Figure 2.1).

The measured intensity $\zeta_{net}(t)$ of the He-Ne laser in the TDFRS experiment used for calculation of the Soret coefficient is:

$$\zeta_{net}(t) = 1 + \frac{(\partial n / \partial x)_{P,T}}{(\partial n / \partial T)_{P,x}} S_T x(1-x)(1-e^{-q^2 Dt})$$

where x is the molar concentration of one of the components, n is the refractive index at the readout wavelength, D is the coefficient of the mutual diffusion and q is the grating vector which has been mentioned before, whose absolute value is determined by the angle θ between two writing beams and the wavelength λ_ω:

$$q = \frac{4\pi}{\lambda_\omega} \sin\frac{\theta}{2}$$

For the determination of the transport coefficients, the measurement of contrast factors $(\partial n/\partial c)_{P,T}$ and $(\partial n/\partial T)_{P,x}$ were done independently.

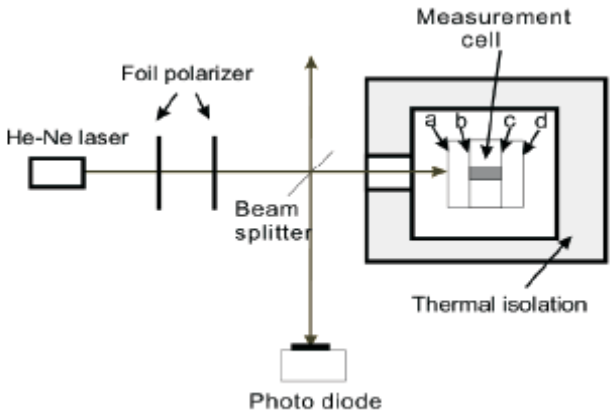

Figure 2.2: Sketch of the $(\partial n/\partial T)_{P,x}$ interferometer (the picture has been taken from previous publication. [5])

The contrast factors $(\partial n/\partial c)_{P,T}$ have been measured by an Abbe refractometer which is operated at 589 nm with further correction for the wavelength of the readout laser (633 nm). The contrast factor $(\partial n/\partial T)_{P,x}$ was measured with a Michelson interferometer at 633 nm. Figure 2.2 shows a drawing of the $(\partial n/\partial T)_{P,x}$-system. To regulate the intensity, two foil polarizers were used. The laser beam was split into two beams. One of them passes through the beam splitter to the measurement cell and is reflected at the windows of the measurement cell. The reflected beams at the front window (**a**, **b**) and at the back window (**c**, **d**) are superimposed at the photodiode. The main contribution of the reflections stem from **a** and **d,** and are due to the larger refractive index differences (≈ 0.5) in air compared to the smaller refractive index differences at **b** and **c** (≈ 0.01) at the inner window, which is in contact with the liquid. The optical path difference s depends on the change of the refractive index n and n_w and on the length l and l_w of the sample and the window, respectively

$$ds = d(nl) + d(2n_w l_w)$$

The temperature derivative of refractive index is obtained by,

$$\frac{\partial n}{\partial T} = \frac{1}{2kl} \cdot \frac{\partial \phi}{\partial T} - 2 \cdot \frac{n_w}{l} \cdot \frac{\partial l_w}{\partial T} - 2 \cdot \frac{l_w}{l} \cdot \frac{\partial n_w}{\partial T} - \frac{n}{l} \cdot \frac{\partial l}{\partial T}$$

For this setup, n_w=1.457. The values of the thermal expansion coefficients $\frac{1}{l_w} \cdot \frac{\partial l_w}{\partial T}$, $\frac{1}{l} \cdot \frac{\partial l}{\partial T}$, and $\frac{l}{l_w} \cdot \frac{\partial n_w}{\partial T}$ are $5.1 \cdot 10^{-7}$ K^{-1}, $7.5 \cdot 10^{-7}$ K^{-1}, and $1.225 \cdot 10^{-6}$ K^{-1}, respectively.[6]

2.3 ***Equilibrium molecular dynamics***.

A molecular dynamics simulation is generated as a trajectory of a set of particles in phase-space. In our studies we worked on an atomistic level, or in other words, atoms are the particles of the system. Molecular dynamics is the bases for calculating the time evolution of the atomic coordinates by solving differential equation numerically. Particles in a system moves under Newton's law of motion. Newton's classical equations of motion for an object as applied to the study of molecular dynamics are given by

$$v(t + \frac{\Delta t}{2}) = v(t - \frac{\Delta t}{2}) + \frac{F(t)}{m} \Delta t$$

$$x(t + \Delta t) = x(t) + v(t + \frac{\Delta t}{2}) \Delta t$$

where $F(t)$ is the force acting on the object, which has mass of m, velocity $v(t)$ and coordinate $x(t)$ at the time of t.

For Newton's equations of motion are to be resolved, therefore, the force acting an each particle has be known and this force can be derived from the interaction potential, which is divided into several contributing components

$$U = U_{non-bonded} + U_{bonded}$$

$$U_{non-bonded} = U_{Lennard-Jones} + U_{electostatic}$$

$$U_{bonded} = U_{bond} + U_{angle} + U_{torsion} + U_{harmonic\_dihedral}$$

The non-bonded interaction $U_{non-bonded}$ is the interaction between two particles i and j. These particles are located apart from each other with a radius smaller than "cut off" (this "cut off" value is established by the experimenter) and defined by:

$$U_{Lennard-Jones} = 4\varepsilon_{ij}[(\frac{\sigma_{ij}}{r_{ij}})^{12} - (\frac{\sigma_{ij}}{r_{ij}})^{6}]$$

$$U_{electostatic} = \frac{q_i q_j}{4\pi r_{ij}\varepsilon_0\varepsilon}$$

where r_{ij} is the distance between the two particles i and j, q_i their charges, ε and ε_0 are the vacuum permittivity and the effective dielectric constant. σ_{ij} and ε_{ij} are Van der Waals parameters for mixed interactions. These can be obtained from the Lorentz-Berthelot mixing rules:

$$\varepsilon_{ij} = \sqrt{\varepsilon_{ii}\varepsilon_{jj}} \qquad \sigma_{ij} = \frac{1}{2}(\sigma_{ii} + \sigma_{jj})$$

where ε_{ii} and σ_{ii} are values which are specific to every type of atom. The potential functions and parameters are typically derived from parameter optimization through comparison to experimental data and quantum calculations. For the optimization of nonbonded parameters, various sources of data can be used, including molecular volumes, experimental heat of vaporization, compressibility and density. In particular, for most of the existing force-field descriptions developed for biomolecules, partial charges on the atoms of a molecule have been determined by ab initio calculations of gas phase complexes with a single water molecule. On the other hand, bonded parameters are usually optimized from experimental data such as gas-phase geometries and vibrational spectra. Bonded items can be defined by the following terms:

Bond Stretch Terms

$$U_{bond} = \sum_{bonds} \frac{k_r}{2}(r - r_0)^2$$

where r is the bond length, r_0 is the equilibrium bond length, and k_r is the force constant.

Angle Bend Terms

$$U_{angle} = \sum_{angles} \frac{k_\varphi}{2}(\varphi - \varphi_0)^2$$

where φ is the angle between two bonds to a common atom, φ_0 is the equilibrium length, and k_φ is the force constant.

Torsion Terms

$$U_{torsion} = \sum_{torsions} \frac{k_\tau}{2}[1 - \cos p(\tau - \tau_0)]$$

For a sequence of three bonds AB, BC, CD along the chain, we define τ as the dihedral torsional angle τ_0 is the equilibrium dihedral torsional angle, p is multiplicity and k_τ is the force constant.

Harmonic dihedrals Terms:

Defines harmonic dihedral angles, similar to torsions, but without periodicity

$$U_{harmonic\_dihedral} = \sum_{harmonic\_dihedrals} \frac{k_\delta}{2}(\delta - \delta_0)^2$$

δ as the harmonic dihedral angle δ_0 is the equilibrium harmonic dihedral angle, k_δ is the force constant.

2.4. *Reverse non equilibrium molecular dynamics (RNEMD)*

In order to calculate the thermal conductivity or Soret coefficient we needed to impose the temperature gradient in our simulation box. This was done using the so-called heat exchange algorithm (HEX).[7] For all simulations we used the YASP package,[8] developed in our group.

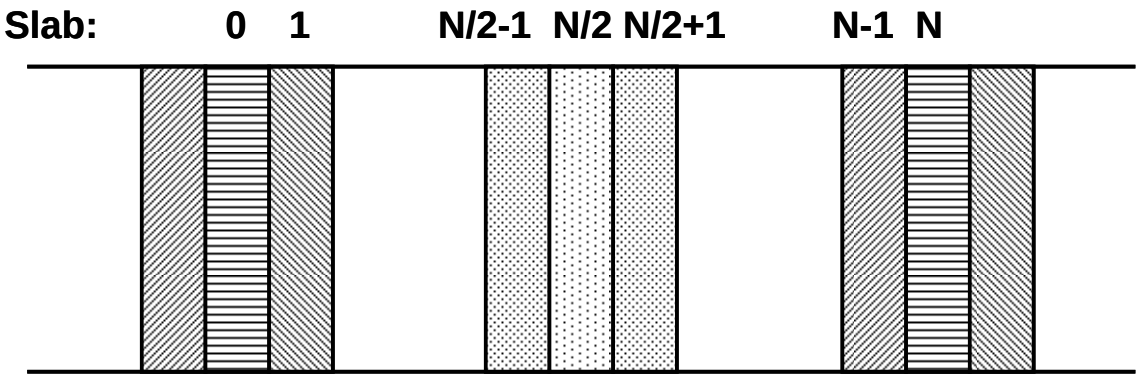

Figure 2.3: Illustration of the heat exchange algorithm for determination of the Soret coefficient by non equilibrium simulation.

In the reverse non-equilibrium algorithm, a heat flux (J_z) is artificially generated through the system by suitably exchanging particle velocities in different regions[5]. The simulation

box is divided into N equal slabs along the z direction (c.f. Fig. 2.3), where slab 0 is defined as "hot" and the center slab N/2 as "cold". Every N_{exch} step, the center-of-mass Cartesian velocity vectors of the "coldest" particle in the "hot" slab and the "hottest" particle in the "cold" slab of similar mass are swapped. Such non-physical velocity exchange produces a physical heat flux in the opposite direction through the intervening slabs (Fig. 2.3), conserving total linear momentum, total kinetic energy, and total energy of the whole system at the same time. The heat flux quantity can be controlled by the exchange frequency, that is, an increased exchange period will decrease the amount of the heat flux. It is defined by:

$$J_z = \frac{1}{2lA} \sum_{transfer} \frac{m}{2} (v_{hot}^2 - v_{cold}^2)$$

where A is the cross sectional area of the simulation box perpendicular, l is the length of the simulation, v_{hot} and v_{cold} are the velocities of the hot and the cold particle of the same mass m, whose velocities are exchanged. On the other hand the heat flux is also equal to

$$J_z = \lambda \frac{dT}{dz}$$

where λ is the capability of the material to transport heat through the system.

For mixtures of molecules the Cartesian centre-of-mass velocity vectors of the two selected molecules need to be exchanged in order to keep their conformations. In this way the relative velocities of all atoms in the given molecule remain unchanged. The Cartesian centre-of-mass velocity vector is defined as

$$\vec{v}_{cm} = \frac{\sum_{\substack{all\_atom\_in \\ molecule}} m_i \vec{v}_i}{\sum_{\substack{all\_atom\_in \\ molecule}} m_i}$$

where m_i and v_i are masses and velocities of atoms in the given molecule. The temperature in a molecular dynamics simulation with constraints is given by the equipartition theorem:

$$\left(\frac{3N - C}{2} \right) k_B T_{slab} = \frac{1}{2} \left\langle \sum_{\substack{\text{atoms } i \\ inslab}} m_i v_i^2 \right\rangle$$

where C is the number of constraints in the slab, N is the number of atoms in the slab, m_i and v_i are the mass and velocity of atom i, and k_B is the Boltzmann's constant.

2.5 *References*

1 D. Reith and F. Müller-Plathe, J. Chem. Phys. **112** (5), 2436 (2000).

2 A. Perronace, C. Leppla, F. Leroy, B. Rousseau, and S. Wiegand, J. Chem. Phys. **116** (9), 3718 (2002).

3 J. K. Platten, M. M. Bou-Ali, P. Costeseque, J. F. Dutrieux, W. Kohler, C. Leppla, S. Wiegand, and G. Wittko, Philos. Mag. **83** (17-18), 1965 (2003).

4 S. Wiegand, J. Phys.-Condes. Matter **16** (10), R357 (2004).

5 P. Polyakov, Ph.D. thesis, University of Twente, Enschede, the Netherlands (2008).

6 G. Wittko and W. Kohler, Philos. Mag. **83** (17-18), 1973 (2003).

7 B. Hafskjold, T. Ikeshoji, and S. K. Ratkje, Mol. Phys. **80** (6), 1389 (1993).

8 F. Müller-Plathe, Comput. Phys. Commun. **78** (1-2), 77 (1993); F. Müller-Plathe and B. P, *Reverse Non-equilibrium Molecular Dynamics*. (2004); F. Müller-Plathe, J. Chem. Phys. **106** (14), 6082 (1997); F. Müller-Plathe and D. Brown, Comput. Phys. Commun. **64** (1), 7 (1991); K. B. Tarmyshov and F. Müller-Plathe, J. Chem Inf. Model. **45** (6), 1943 (2005).

Chapter 3: Anisotropy of the thermal conductivity in a crystalline polymer: Reverse non-equilibrium molecular dynamics simulation of the δ phase of syndiotactic polystyrene

3.1. Introduction

Technical applications of polymers are often determined by their thermal properties. Design goals can be a particularly low thermal conductivity, for example in thermal insulation, as well as a particularly high thermal conductivity, for example in the packaging of electronic devices. High conductivities are often achieved in practice by blending the polymer with highly conductive inorganic fillers. An alternative is the use of polymer materials which are intrinsically better heat conductors, such as semicrystalline polymers with a high degree of crystallinity. Polymer crystallites are generally assumed to conduct heat better than the amorphous regions, both because of their higher density and the possibility of fast heat transport by phonons.

The thermal conductivity of crystalline polymers is also of fundamental scientific interest. It will be anisotropic, and the conductivity along the polymer chains (phonon mechanism) is likely to be faster than perpendicular to it (collisions between atoms or groups of neighbouring polymer chains). Or, in other words: parallel to the chain direction, the transport will be more solid-like, whereas perpendicular to the chains, it will have a larger liquid-like component. Amorphous polymers, too, have both transport mechanisms, but they are difficult to separate. Thus, crystalline polymers can serve as separable model systems for studying the heat-transport mechanism in polymers in general. In polymer crystals, many properties show anisotropies: mechanical properties, transport properties, as well as others. Some have already been studied by molecular simulation, for example the anisotropic diffusion of small penetrants in crystalline polystyrene[1] and poly(4-methyl pentene)[2] and the anisotropy of the thermal expansion of different crystalline polymers.[3]

We chose to investigate the thermal conductivity and, in particular, its anisotropy in polymer crystals by molecular dynamics simulations. The reasons are: (i) In simulations, the systems are well defined. The crystals are clean and perfectly oriented,

so heat conduction along the different crystal axes can be unambiguously distinguished. (ii) With the reverse non-equilibrium molecular dynamics method, we have a robust tool for obtaining the diagonal elements of the thermal conductivity tensor.[4] This method has already been applied to molecular fluids[5] and amorphous polymers.[6] (iii) We have already investigated the anisotropy of heat conduction in stretched amorphous polyamide-6,6 by this method.[7] One result was that the thermal conductivity in the stretching direction is enhanced over the unstretched amorphous sample, whereas in the perpendicular directions it was decreased. Turning from an amorphous stretched polymer to a polymer crystal should generate an even larger anisotropy.

The crystalline polymer investigated here is crystalline syndiotactic polystyrene (sPS). The reasons for this choice are partly convenience (we have simulated this polymer in another context before and therefore have tested force field parameters[1]), partly the representative character of this polymer (the majority of crystalline polymers forms helices like sPS), and partly its technical and scientific importance (the low-density δ modification has cavities which can accommodate small molecular guests[8]). No individual components of the thermal conductivity tensor seem to be available from experiment for any crystalline polymer. Syndiotactic polystyrene is no exception. Hence, only the experimental thermal conductivity of syndiotactic polystyrene with unknown crystallinity can provide an order-of-magnitude estimate of the thermal conductivities to be expected.

Syndiotactic polystyrene has another feature, which makes it interesting as a model system for a first study. Its δ phase is a loosely-packed crystal. Its density of 0.977 g/cm^3 [1] is even lower than that of the amorphous syndiotactic polymer (1.055 g/cm^3). The phase is metastable, and upon heating it spontaneously converts to the denser α or β crystalline phases.[9] This metastability is also observed in the molecular-dynamics simulations. We find that a collapse of the δ structure to a denser crystal structure can easily be induced. While this compact structure is not a proper α or β phase, it still serves as a comparison to study the effect of an increase of the number of degrees of freedom per volume on the thermal conductivity and its anisotropy.

In addition to the anisotropy in polymer crystals, we study the effect of the computational model or force field on the thermal conductivity. It has been found for molecular liquids[5] and for amorphous polyamide-6,6[7] that for a faithful description of the thermal transport not all *intra*molecular degrees of freedom may be retained in the model. It has been suggested that in reality the fast vibrations, such as bond stretching, are quantum oscillators and not excitable at room temperature. They can, therefore, not contribute to the storage and transport of energy. In a classical mechanical simulation, they should be removed from the force field and substituted by bond constraints or united atoms. Otherwise they can lead to artificially high simulated thermal conductivities. As this observation is so far only based on but a few examples, we continue this investigation in the present contribution by studying the influence of different constraint patterns on the thermal conductivity.

3.2. Methods

The reverse non-equilibrium molecular dynamics (RNEMD) method has been established as a robust way of calculating thermal conductivities of liquids and polymers.[4-7] It has been described in every detail, including its strengths and weaknesses,[10] so that only a short summary is given here. It assumes linear response, i.e. Fourier's law

$$J_z = -\lambda(\frac{dT}{dz}),$$

where J_z is the heat flux in one direction (here: z direction) and (dT/dz) is the temperature gradient in the same direction. The proportionality constant λ is the thermal conductivity. In contrast to experiment, the heat flux is artificially imposed on the system and the temperature gradient is obtained from the temperature profile resulting in the system, whence the attribute "reverse". The periodic simulation cell is divided along the z direction into $N_s = 12$ slabs of identical volume; the first slab is designated as the "hot"

slab and the central slab ($N_s/2$) as the "cold" slab; energy is periodically transferred unphysically from the cold slab to the hot slab. As energy is conserved, it flows back through the system in the *z* direction by a physical transport mechanism, resulting, at steady state, in a temperature profile.

The artificial heat flow is maintained by exchanging momenta of suitably selected particles, typically the hottest (=fastest) particle in the cold slab with the coldest (=slowest) particle in the hot slab. In its simplest form, the algorithm exchanges momenta of individual atoms ("atomic exchange"). If the algorithm is used in connection with bond constraints, it is, however mandatory, to avoid constraint violations by the momentum exchange. Therefore, momenta of the centres of mass of entire molecules ("molecular exchange" for molecular fluids and fluid mixtures) or of substructures of molecules ("semimolecular exchange" for macromolecules) are exchanged. These semimolecular groups may internally contain constraints. The chemical bonds between them must, however, be modelled by flexible bond terms. As constraints are needed in this work for physical reasons, we make much use of the semimolecular exchange. Details of the various exchange schemes can be found in refs. 7 and 10.

3.3. Computational Details

The initial coordinates of the δ modification of sPS were taken from the work of Milano et al.,[1] which is based on the experimental X-ray structure.[11] The basic cell contained several unit cells with altogether 12 polystyrene chains (Figure 3.1). Every chain had 16 monomers. Periodic boundary condition acted in all directions, so that the last backbone carbon of a chain was connected to the periodic image of its first backbone carbon. Thus, the system simulated corresponds to the limit of a perfect polymer crystal, which is infinite in all dimensions, including in the chain direction. There were no chain ends in the simulation, and the study of crystal faces, finite or broken chains, chain defects and the like is beyond the scope of this contribution. The basic cell was replicated three or four times in the direction of the heat flow (Figure 3.2). For a study of the thermal conductivity component in *z* direction for example, there were thus 12 chains of

48 monomers each in the final simulation cell, again with periodic boundary conditions in all directions.

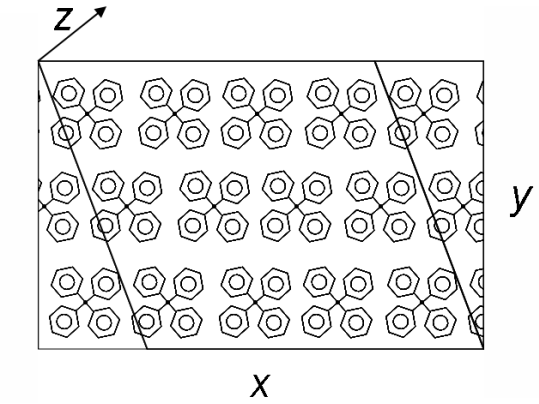

Figure 3.1: The δ modification of syndiotactic polystyrene (sPS) viewed along the helix axis (*z* direction).

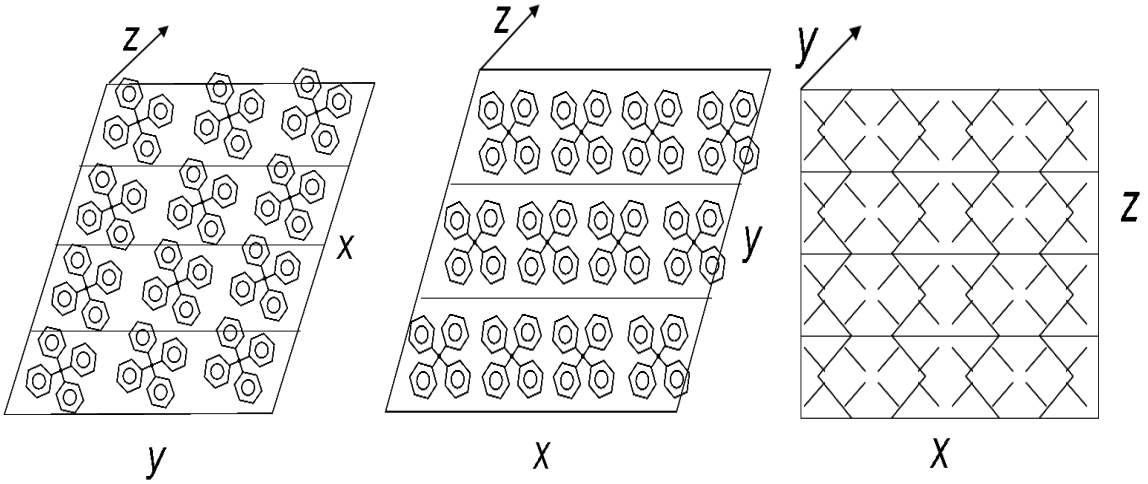

Figure 3.2: Different projections of the basic cell and its division into analysis slabs in *x*, *y* and *z* directions, respectively. For the RNEMD simulations, the basic cell has been replicated in the direction of the temperature gradient and heat flow: 3 times in *x* and *z*, 4 times in *y* direction, respectively.

The polystyrene force field has been used before in our work [1,12]. It was augmented, where necessary, with harmonic force constants for those bonds, which were

not constrained (see below). The force constant was 360000 kJ mol^{-1} nm^{-2} for aromatic C-H bonds and 420000 kJ mol^{-1} nm^{-2} for all other bonds. The constrained bonds were kept rigid by the SHAKE algorithm.[13,14] As there has been a systematic influence of the number and of degrees of freedom on the calculated thermal conductivities in our previous studies,[5,7] different constraint patterns were tried. They are visualized in Figure 3.3. The force field includes atomic partial charges on the phenyl rings. For the electrostatic interactions, the reaction field method has been used with a dielectric constant of 2.5.

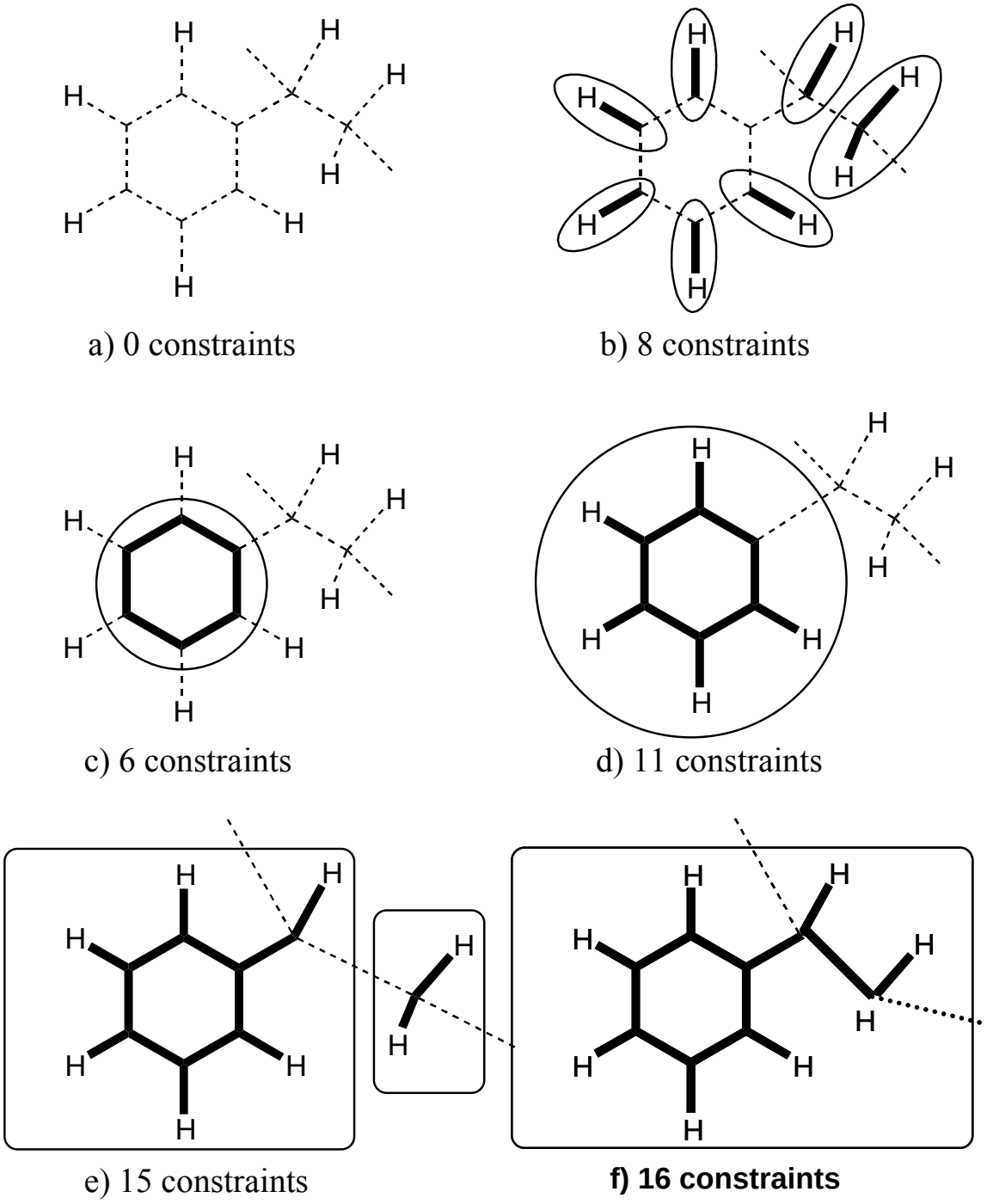

Figure 3.3: Scheme of the different constraint patterns and assignment of semimolecular groups. Constrained bonds are marked by thick solid lines, flexible bonds by thin dashed lines. Semimolecular groups of atoms are encircled.

All simulations were performed by the program YASP[15,16]. The time step was 0.0005 ps. The nonbonded cutoff was 1.1 nm for the neighbour list and 1.0 nm for the interactions. The neighbour list was updated every 15 time steps. The average temperature of the system was kept at 300 K using the Berendsen method with a coupling time of 0.2 ps .[17] (In the nonequilibrium simulations, only the temperature averaged over the simulation box is thereby held fixed, while the RNEMD scheme in steady state leads to a constant temperature gradient and, hence to a local variation of the temperature.) In the equilibrium simulations only, also the pressure was kept at 101.3 kPa by a Berendsen manostat with a coupling time of 10 ps. For every system, equilibration was performed for at least 10 ns. After this period, the fluctuations of total energy and density over 500 ps were in all cases below 2%.

For the non-equilibrium (RNEMD) simulations, the system was divided into 12 equal slabs along the *x*, *y*, or *z* direction. This number of slabs for the calculation of thermal conductivities is the result of the following considerations. There have to be enough slabs for the temperature gradient to be reasonably well defined. On the other hand, it turned out that, in a crystalline system, the number of slabs should be commensurate with the crystal structure. If this is not the case, the temperature gradient ($dT/d\alpha$, $\alpha=x,y,z$) can show spurious non-linearities as a consequence of equally spurious density oscillations. For an incommensurate division into slabs, an artificial density variation of more than 10% and a concomitant nonlinearity of the temperature gradient are evident (Figure 3.4). This problem had hitherto not been encountered in our previous thermal conductivity calculations for molecular liquids and amorphous polymers. To avoid such artifacts, we have always used 12 analysis slabs and ensured that in the transport direction investigated, there were either 12 layers of polymer helices in that direction (*x* and *y*) or 48 (=4×12) monomers per chain (*z*), cf. Fig 3.2. Momentum exchange between equal atoms or semimolecular groups has been performed every 900, 1100 and 500 steps for the calculation of the thermal conductivity component in the *x, y* and *z* direction, respectively. The selection of these values is based on two requirements. On the one hand, the velocity exchange rate has to be large enough for fast convergence

of the temperature profile. On the other hand, a too large perturbation causes the hot slab to heat up so much, that the transition of the metastable δ phase to the collapsed structure can be induced. This is to be avoided. The chosen velocity exchange rates are a compromise worked out by trial and error. They cause temperatures between 318 and 325 K on the hot side. The exchange rates are different for the different directions, because the thermal conductivities are different: For a certain maximum temperature not to be exceeded in the simulation, a higher heat flux (larger exchange rate) is allowed if the thermal conductivity is larger.

The RNEMD calculations were run for at least 1 ns, until the steady state was reached. They were continued for at least another 0.25 ns for sampling the temperature profile: The temperature profile and the imposed heat flux were sampled every 901^{th}, 1101^{th} or 501^{th} step, respectively. The calculations were performed under constant-average temperature and constant volume conditions, with the same coupling times as in the equilibrium simulations, see above.

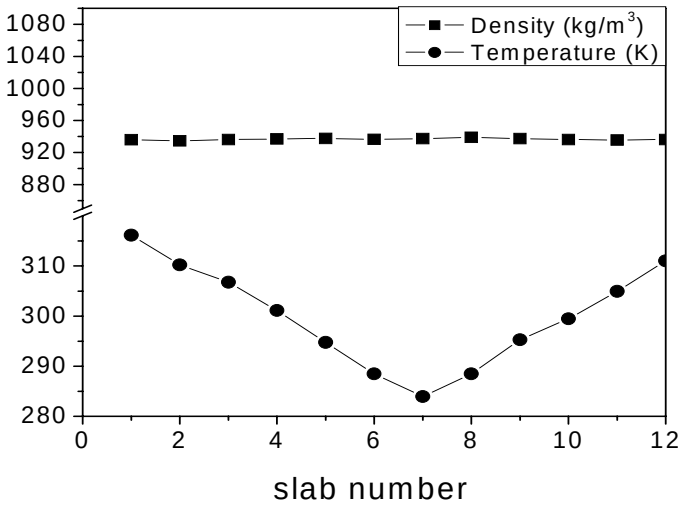

Figure 3.4a

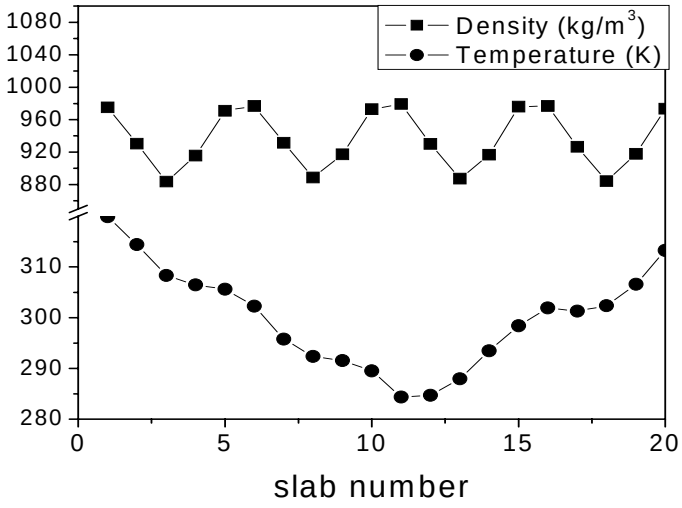

Figure 3.4b

Figure 3.4: Density and temperature profiles of the same system (temperature gradient and heat flux in *z* direction, time step 0.0005 ps, semimolecular velocity exchange every 0.25 ps, 8 constraint (Figure 3.3b), the average temperature of the system is 300K, which for the RNEMD analysis has been divided into different numbers of slabs: (a) 12 slabs, which is commensurate with the 48 monomers/chain in this direction: (b) 20 slabs, which is incommensurate and leads not only to spurious density oscillations, but also to nonlinearity artefacts in the temperature profile.

From the error bars of the heat flux J and the temperature gradient $S = (dT/dz)$, the error bar $\Delta\lambda$ of the thermal conductivity λ has been calculated by error propagation

$$\Delta\lambda \le \lambda\left(\frac{\Delta J}{J} + \frac{\Delta S}{S}\right)$$

The temperature gradient and its error bar ΔS have been determined by a least-squares fit to the temperature profile (as in Figure 3.4a). For an error estimate of the heat flux ΔJ, we calculated the cumulative exchanged energy. In the steady state, it is linear in the simulation time with a slope J. From a least-squares fit, the error ΔJ was extracted.

The use of periodic boundary conditions in the MD simulation precludes the existence of certain phonons, especially those whose wavelengths exceed the length of the simulation box. Such long-wavelength phonons may contribute to static and dynamic properties, especially, in crystalline phases. To check for possible contributions of long-wavelength phonons to the thermal conductivity of the δ phase, it has been recalculated with a box two times larger in the direction of the applied thermal gradient. No constraints have been used. The simulation cells have been divided into 24 slabs (2*12 slabs). The velocity exchange has been performed every 5000, 7000 and 2000 steps, for the different directions, respectively. The perturbation is thus smaller than in the small systems. This was done as a safeguard against a possible temperature-induced collapse of the metastable δ phase, which is more likely to occur in the larger systems. Table 1 shows that all Cartesian components of the thermal conductivity agree within their error bars for both sizes, indicating that there are no finite-size effects on the scales investigated here. Effects on the thermal conductivity, however, unlikely, would have to come from phonons of much longer wavelengths.

Table 3.1: Components of the thermal conductivity in the Cartesian directions [W m^{-1} K^{-1}] calculated for a simulation cell with the standard size of this work and with twice the size in the respective direction of thermal gradient.

	size used in this work	Double size
λ_x	0.171 ± 0.005	0.177 ± 0.006
λ_y	0.224 ± 0.004	0.226 ± 0.005
λ_z	0.554 ± 0.012	0.537 ± 0.023

3.4. Results and Discussion

3.4.1. Metastability of the δ modification of syndiotactic polystyrene

The δ modification of sPS has an unusually low density and is known to be metastable. It can only be produced in the presence of small guest molecules, which occupy and stabilize its intrinsic cavities. Upon annealing, it spontaneously converts into the denser α or β forms. This behaviour was also found in some of the simulations, in which the δ crystal spontaneously collapsed into a denser structure. This collapse was always irreversible. In the dense structure, which we denote as "compact", the helices are still intact. (If they had a tendency to disintegrate or unravel or change sense, this would be effectively prevented by the small system size and the periodic continuation of the chains. Hence, such structural change would not be seen in our simulations even if were thermodynamically favorable.) The density increased from around 0.975 g/cm^3 of the δ modification (experiment 0.977 g/cm^3)[18] to about 1.091 g/cm^3. This density is above the experimental value for amorphous sPS (1.055 g/cm^3)[11] and close to the experimental density (1.09 g/cm^3)[19] of the α and β modifications. However, the compact structure is different from the crystal structures of the α or β phases of sPS. We suspect that we observed the initial compaction of the metastable δ-sPS crystal, whilst the final rearrangement to one of the other crystal structures is either kinetically slow or is effectively hindered by system size and periodic boundary conditions, see above. The densities of the δ modification and of the compact form do not depend significantly on the constraining patterns (Table 3.2).

Table 3.2: Components of the thermal conductivity in the Cartesian directions [W m^{-1} K^{-1}], cell dimensions [nm], and densities [g/cm^3] for syndiotactic polystyrene (300 K) and the different constraint patterns (cf. Figure 3.3): (a) δ phase; (b) compact structure.

a) δ phase

		0 constraints	8 constraints	6 constraints	11 constraints	15 constraints	16 constraints
λ_x		0.171 ± 0.005	0.162 ± 0.001	0.156 ± 0.004	0.155 ± 0.005	0.172 ± 0.007	0.107 ± 0.004
λ_y		0.224 ± 0.004	0.198 ± 0.001	0.207 ± 0.002	0.184 ± 0.004	0.200 ± 0.004	0.186 ± 0.004
λ_z		0.554 ± 0.012	0.475 ± 0.025	0.523 ± 0.010	0.512 ± 0.024	0.510 ± 0.027	0.301 ± 0.014
Dimension	*X*	3.319	3.318	3.319	3.319	3.318	3.319
	Y	3.309	3.307	3.309	3.309	3.308	3.308
	Z	3.102	3.101	3.102	3.102	3.103	3.102
Density		0.974 ± 0.003	0.975 ± 0.002	0.974 ± 0.002	0.974 ± 0.002	0.974 ± 0.002	0.974 ± 0.003

b) compact structure

		0 constraints	8 constraints	6 constraints	11 constraints	15 constraints	16 constraints
λ_x		0.234 ± 0.002	0.205 ± 0.004	0.207 ± 0.004	0.204 ± 0.004	0.203 ± 0.007	0.171 ± 0.01
λ_y		0.251 ± 0.003	0.223 ± 0.006	0.226 ± 0.002	0.221 ± 0.007	0.231 ± 0.011	0.183 ± 0.006
λ_z		0.510 ± 0.008	0.501 ± 0.009	0.468 ± 0.012	0.474 ± 0.013	0.544 ± 0.087	0.339 ± 0.011
Dimension	*X*	3.198	3.198	3.202	3.201	3.195	3.193
	Y	3.189	3.189	3.183	3.182	3.185	3.179
	Z	2.989	2.989	2.993	2.991	2.985	2.986
Density		1.089 ± 0.011	1.090 ± 0.010	1.088 ± 0.018	1.093 ± 0.012	1.097 ± 0.015	1.096 ± 0.017

In the context of calculating thermal conductivities for crystalline sPS, there are two consequences from the tendency of the δ modification to turn into the compact form. Firstly, if we want to calculate properties of δ-sPS, we must make sure that this modification exists throughout the simulation. It turned out that the occurrence of a

compaction depends on the details of the simulation. The length of the time step has an influence as does the constraint pattern. There seems to be a delicate balance, which keeps the δ form metastable and a small disturbance tips the system over the edge to compaction. Some combinations (e.g. time step = 0.002 ps and constraint pattern of Figure 3.3e) led to a compaction within 10 ns, whereas others (e.g. time step = 0.0005 ps and constraint pattern of Figure 3.3c) showed (meta)stability over the entire simulation of 50 ns and longer. We have, therefore, continued our simulations with the latter time step. It should also be noted that the collapse of the δ phase had not been observed in our previous simulations of this system.[1] This may be due to the fact that in those simulations there were small guest molecules present, which stabilized the structure. Alternatively, the previous simulations may simply have been too short for a compaction event to happen. Secondly, even though the thermodynamic state and the experimental relevance of the compact structure are not clear, we have nonetheless calculated its thermal conductivities. These values act as reference points for understanding the effects of density on the thermal conductivity and its anisotropy.

3.4.2. Magnitude of the thermal conductivity

There seems to be no experimental information available for the thermal conductivity of crystalline syndiotactic polystyrene in any of its modifications. A sample of semicrystalline syndiotactic polystyrene of unknown crystallinity at 300 K (density 1.050 g/cm^3) showed a thermal conductivity of 0.19±0.03 W m^{-1} K^{-1}.[20] It is to be expected that the average thermal conductivity of crystalline sPS is larger, but of the same order of magnitude. This was indeed found for the different models (Table 3.2): The calculated average thermal conductivity $\overline{\lambda} = \left(\lambda_x + \lambda_y + \lambda_z\right)/3$ is between 0.20 and 0.30 W m^{-1} K^{-1} for the δ form and between 0.23 and 0.33 W m^{-1} K^{-1} for the compact form, with variations depending on the constraint pattern. This level of agreement shows that our models are in the right order of magnitude. The agreement is consistent with our recent study on polyamide-6,6,[6,7] where the calculation and the experiment agreed to within a factor of 1.0-1.5, depending on the model.

It is interesting to note that the difference between the average thermal conductivity of the δ modification and the compact structure is approximately proportional to their density difference (~11%.). The thermal conductivity is, therefore, approximately proportional to the number of degrees of freedom (which are the transporters of heat) per volume. If this reasoning holds, the α and β modifications, which have densities similar to the compact form, may be expected to also have similar average thermal conductivities. This speculation can, however, only be verified or falsified by experimental measurements.

3.4.3. Anisotropy of the thermal conductivity

For both structures, the heat transport in the helix direction (z) is much larger than in the perpendicular directions (Table 3.1). The anisotropy defined as $2\lambda_z/(\lambda_x + \lambda_y)$ is about 2.7 (2.0-3.0 depending on the constraint pattern) for the δ form and about 2.1 for the compact form. The decrease from δ to compact is due to both a decrease of the parallel component λ_z and an increase of the two perpendicular components, in particular λ_x. This is shown numerically in the anisotropy between the two perpendicular thermal conductivities λ_y/λ_x. This ratio is about 1.32 for the δ modification, and it drops to about 1.09 for the compact form. This could be again a hint, that the more compact crystal modifications α and β could have a reduced anisotropy (helix direction versus perpendicular directions) and that the two perpendicular directions could be very similar.

Looking at the structure (Figure 3.1), one would naïvely expect a higher thermal conductivity in x direction than in y, because of the apparently smaller distance between the chains in x direction. The opposite is true: λ_y is higher than λ_x. The reason is a closer contact between atoms of opposite phenyl rings in y direction, which has been observed in a crystal structure by de Rosa et al..[18] The shorter overall distance between pendant groups arises from a shorter distance in z direction, which is not visible in the two-dimensional projection of Figure 3.1.

The change of the individual thermal conductivity components with the transition from the δ modification to the compact structure can be understood by inspection of the

polymer structure shown in Figure 3.1. Most of the density increase is caused by compaction perpendicular to the helix direction *z*. Thus, neighbouring chains get into closer contact in these directions. As a consequence, λ_x and λ_y, which are mainly determined by collisions of atoms of neighbouring chains, increase. The heat transport in the direction parallel to the helix λ_z remains largely unchanged by compaction. It shows only small increases or decreases depending on the constraint pattern. The reason for this behaviour is that the heat conduction in helix direction includes a larger component of (faster) phonon transport than in the perpendicular directions. This transport proceeds largely unhindered in a polymer helix, which is free of internal defects. The change of the environment of the individual helix due to closer packing with its neighbours provides only a small perturbation to the heat transport within the chain. It leads only to small increments or decrements of the thermal conductivity λ_z.

3.4.4. Influence of constraint patterns on the thermal conductivity

In previous work, was been found that the number of degrees of freedom of a model has an influence on the calculated value of the thermal conductivity. Degrees of freedom store the energy and transfer it. Eliminating explicit hydrogen atoms by united-atom models as well as using constraints decreases the number of available degrees of freedom and consequently decreases the thermal conductivity. This tendency was not only found for molecular fluids[5], but also in an almost quantitative correlation for different models of amorphous polyamide-6,6.[6,7] According to these considerations, the thermal conductivity of the different sPS models is, therefore, expected to decrease for an increasing number of constraints. Table 3.2 shows that this is clearly not always the case.

One observes, firstly, that the variations due to the constraint pattern are relatively small: For a given polymer structure and thermal conductivity component, different constraint patterns cause differences of about 32%. This has to be compared to almost a factor of 2 in the case of polyamide-6,6.[7] So it appears that the thermal conductivity of crystalline sPS is remarkably robust against variation of the degrees of freedom in the model. This is advantageous for the reliability of the predictions. Secondly, there is no

systematic variation of the thermal conductivity with the number of constraints. One may interpret into the data a general trend of the thermal conductivity falling with the number of degrees of freedom. This trend is, however, superposed by erratic variations: For example, the λ_x of the δ phase decreases from 0 to 6 constraints, then increases at 8 constraints, falls again at 11 constraints, before increasing at 15 constraints where the highest conductivity of all is found. However, the 16-constraints model always shows the smallest thermal conductivity. Especially for the parallel direction, it is significantly below all other constraint patterns.

The observations (small variations, erratic variations, and the 16-constraint model being systematically below the others) can probably be explained by the fact that not only the number of degrees of freedom matters for the heat transport, but also their location. Some of the C-C bonds in the backbone have to be treated as flexible, as otherwise the breakdown of the polymer into the semimolecular groups of the RNEMD algorithm would not be possible. In the first five constraint patterns (constraints < 16), these bonds of the main chain are treated as flexible bonds with high vibrational frequencies. On the other hand, these backbone bonds are responsible for most of the heat transport along the polymer chain. Freezing one half of them (16 constraints) leads to the observed significant reduction of the thermal conductivity. In contrast, the pendant atoms and groups are not strongly coupled to the energy transport along the backbone, and it is not important whether or not they contain a few constraints. In contrast, in polyamide-6,6 there are no large pendant groups and the constraint patterns studied in ref. 4 involved also a substantial fraction of backbone bonds. It is, therefore, in hindsight no surprise that for polyamide there was a strong correlation between the number of degrees of freedom and the thermal conductivity, whereas in the polystyrene of the present work the correlation, if any, is much weaker.

3.4.5. Influence of chain packing on the thermal conductivity

Differences in the density, or the density of degrees of freedom per volume, have already been made responsible for differences in the thermal conductivity of the δ

modification of sPS and the compact form (Sect. 3.4.2). In order to study the effects of density or chain packing in more detail, we have performed additional simulations of both forms, in which only the density was varied, while the respective crystal structure was left intact. This should allow the separation of the effects of density and that of other structural differences between the two phases. For this comparison, we have chosen the completely unconstrained model of sPS (0 constraints, Figure 3.3a). The volume of the simulation cell has been varied by changing only the dimensions x and y, which are perpendicular to the chain direction. The z direction has been kept constant, assuming that the chains are inherently stiff in this direction, and that a change of the cell length in z may only be achieved at the expense of a structural transition of the polymer helices, i.e. other crystalline or amorphous phases. The x and y components of the cell dimensions and the atom coordinates were affinely scaled by a common factor P with respect to their average values obtained from equilibrium simulations (300K and 101.3 kPa). The cell volume V after scaling is, therefore, $V = P^2 V_0$, where V_0 is its equilibrium volume. The density of degrees freedom is now P^{-2} times its equilibrium value at standard temperature and pressure (or: $P^{-2} = \rho/\rho_0$, with ρ_0 being the density at equilibrium). The simulations with the scaled volume were run under constant-volume conditions.

The scale factor P has been set to 0.965, 0.97, 0.98, 0.99, 1.01, 1.02 and 1.03, both for the δ form and the compact form. The resulting thermal conductivity components are shown in Figure 3.5 as a function of the relative density ρ/ρ_0. Changing the size of the x and y dimensions by a few percent has only a small bearing on the heat conductivity of both structures. Furthermore, there are not only differences between the two structures, but different directions of the heat flux are affected in different ways. Thus, it makes sense to discuss separately the heat transport parallel to the helix direction (z) and perpendicular to it (x and y).

For the parallel heat conductivity λ_z, recall that the thermal conductivity is defined as the amount of energy transported in z direction per time, per temperature gradient, and per cross-sectional area $L_x \times L_y$. As $L_x \times L_y$ is proportional to P^2, λ_z is expected to be proportional to $P^{-2} = \rho/\rho_0$ when there are no other effects. This is evidently not always the

case (Figure 3.5). While for the δ modification one might argue about the presence of a linear increase of λ_z with ρ/ρ_0 (Figure 3.5a), for the compact form there is definitely a decrease (Figure 3.5b). There is some logic to this finding. In the loosely-packed δ form, individual helices are more decoupled in their heat transport, and compressing them in a perpendicular direction has only the geometric effect of increasing the number of chains per cross-sectional area. In contrast, in the compact structure the closer packed neighbouring chains interfere negatively with each other's transport by disturbing long-wavelength phonons; lateral compression enhances these interferences, and the thermal conductivity λ_z decreases. The stronger mutual influence of neighbouring chains in the compact configuration is evident from the mean-square fluctuation of the backbone carbon atoms as a function of ρ/ρ_0. For the compact structure, the dependence (slope) is much larger than for the loosely-packed δ modification (Figure 3.6).

Turning to the heat transport perpendicular to the chain directions λ_x and λ_y, scaling of L_x and L_y by P means that both the cross-sectional area is changed (this time by P, not P^2), but also the dimension of the system in the direction of the transport, equally by P. The expected geometric effect is an increase of λ_x (or λ_y) as $P^{-1} = \sqrt{\rho/\rho_0}$. Any deviation from this behaviour would first and foremost have to be attributed to the extension or compression of the system in the direction of heat flow, i.e. perpendicular to the chain direction. The behaviour in Figure 3.5 is mixed. For the loosely-packed δ form (Figure 3.5a), there is an increase of λ_y with ρ/ρ_0; whether square-root or linear or some other law may be argued about. The other perpendicular component λ_x is definitely independent of ρ/ρ_0. For the compact form (Figure 3.5b), there is a clear increase (most likely linear) with ρ/ρ_0 for both perpendicular components. An explanation relies again on the higher density of the compact form. Here, the neighbouring chains are in close contact, and changing their contact distances has a pronounced effect on the perpendicular heat transfer from chain to chain. The result is a dependence, which is stronger than from geometrical considerations alone. In the looser δ form, the effect of the chain-chain distance is not so large, and the dependence of λ_y largely follows the geometry. The observed reduction of λ_x with ρ/ρ_0 must have still more subtle reasons.

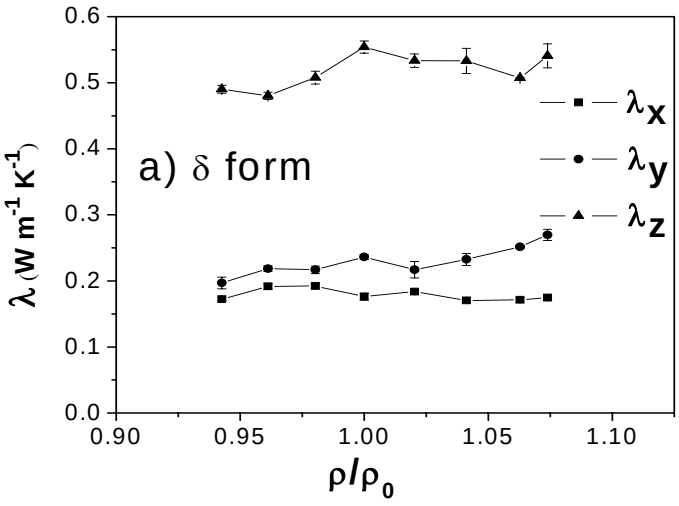

Figure 3.5a

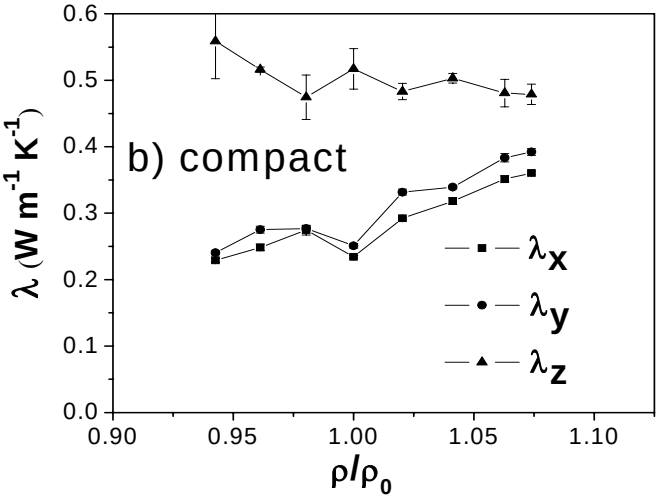

Figure 3.5b

Figure 3.5: Thermal conductivity (Cartesian components) of sPS at 300 K as a function of the density normalized by its equilibrium value at 300 K and 101.3 kPa: (a) δ form, and (b) compact form

A final remarks concerns possible inhomogeneities of the stress in the system. A large enough temperature gradient can induce a density gradient, particularly in

molecular fluids. In polymers, in contrast, chain connectivity keeps density differences much smaller. This is evident, for example, in Figure 3.4. There could, however, be local differences in the stress, which we have not investigated. They could possibly lead to locally varying shifts in effective vibrational frequencies and thus have an effect on the thermal conductivity. We expect such effects to be small. The density variations discussed here have concomitant stress variations, which are probably larger than those induced by a thermal gradient. And even they have not produced significant effects on the thermal conductivity. The problem of stress inhomogeneities affecting the thermal conductivity would merit its own investigation, probably with a simple model system rather than a realistic polymer model, and it would most likely need much longer simulations to distinguish an effect above the statistical noise.

3.5. Summary

The main purpose of this chapter is to investigate, for the first time, the thermal conductivity in a polymer crystal and the anisotropy between its individual Cartesian components by non-equilibrium molecular dynamics. To this end, the δ modification of syndiotactic polystyrene (sPS) was simulated, which is of low density and metastable, as well as a more stable, so-called compact structure, which has a density similar to the crystalline α and β forms of sPS, but not their crystal structure. The overall thermal conductivities have been found to be in the correct range, with experimental thermal conductivities not available for these systems: Comparison of the absolute values with the thermal conductivities of amorphous polymers and, especially, amorphous syndiotactic polystyrene show the expected level of agreement.

The crystalline structure of the polymer causes the thermal conductivity to be anisotropic. Reverse non-equilibrium molecular dynamics can clearly differentiate between the diagonal components of the thermal conductivity tensor. The heat conduction parallel to the polymer chains λ_z is 2.5–3 times faster than perpendicular to it, λ_x and λ_y. This finding tallies with our previous results on oriented but still amorphous polyamide-6,6, where we also found the largest thermal conductivity in the stretching

direction.[6,7] The reason is in both cases that different heat conduction mechanisms dominate different spatial directions. Along the chain (z), there is a strong coupling of stiff and nearly harmonic degrees of freedom and the energy transport proceeds via phonons. Perpendicular to the chain direction (x and y), heat has to be transferred between atoms of neighbouring chains by a less efficient mechanism. The lower efficiency arises from the softer coupling and the strong anharmonicity of intermolecular interactions. Although technically the perpendicular motions of polymer segments in a crystal can be denoted as transversal phonons, the mechanism of energy transfer between chains is much more akin to the collision transfer mechanism, which dominates heat conduction in liquids. The two perpendicular directions show between them a small difference in their thermal conductivities λ_x and λ_y. This residual anisotropy can be explained by closer contacts between pendant groups of adjacent chains in one of the directions. Compaction of the crystal from the δ phase to the compact structure has the expected effects: The perpendicular thermal conductivities λ_x and λ_y increase due to closer contact between neighbouring chains. The parallel thermal conductivity λ_z does not change much. If anything, it shows a slight decrease, possibly due to perturbation or scattering of phonons by the interaction with the neighbouring chains. These interpretations are also borne out by the comparison, in terms of thermal conductivities, of structures which are slightly compressed or expanded, but still in their original crystal phase.

The influence of the constraint patterns on thermal conductivity was also examined. Lo and behold, we found an increase of the thermal conductivity with the number of degrees of freedom or the number of unconstrained bonds, albeit with a considerable scatter of the data. In contrast to our previous simulations on molecular liquids and amorphous polymers[5,6], where we found a clear correlation, in both crystalline sPS structures the dependence is not as pronounced. The one exception are the backbone bonds: If they are constrained the thermal conductivity is visibly reduced. This observation is another indication that the dominant energy flow in polystyrene occurs via the backbone. The degrees of freedom of the pendant phenyl rings make only a minor

contribution. Therefore the constraints within the side groups matter less. This is different in the polyamide studied previously, which has no significant side groups, such that all degrees of freedom have a more or less equal role in the energy transport. These preliminary conclusions are, however, based on a very limited statistic of two polymers. Studies on other polymers with different chemical connectivities are under way to investigate the correlation between degrees of freedom and the thermal conductivity in more detail.

From an application point of view, it is interesting to note that the average thermal conductivity $(\lambda_x + \lambda_y + \lambda_z)/3$ of the polymer crystal is larger than that of the amorphous polymer with the same chemistry λ_a. The reason is that the component along the chain is increased significantly; here, λ_z is 2.5–3 times larger than λ_a. The perpendicular components, on the other hand, are of a similar magnitude as the amorphous thermal conductivity, $\lambda_x \sim \lambda_y \sim \lambda_a$. In summary, a net increase results from crystallization. Crystallization, thus, opens a way of increasing the intrinsic thermal conductivity of a polymer material without the addition of heat-conducting inorganic filler particles.

3.6. References

[1] G. Milano, G. Guerra, and F. Müller-Plathe, Chem. Mat. **14** (7), 2977 (2002).

[2] F. Müller-Plathe, J. Chem. Phys. **103** (10), 4346 (1995).

[3] R. Martonak, W. Paul, and K. Binder, J. Chem. Phys. **106** (21), 8918 (1997); J. D. Carbeck and G. C. Rutledge, Polymer **37** (22), 5089 (1996).

[4] F. Müller-Plathe, J. Chem. Phys. **106** (14), 6082 (1997).

[5] M. M. Zhang, E. Lussetti, L. E. S. de Souza, and F. Müller-Plathe, J. Phys. Chem. B **109** (31), 15060 (2005).

[6] T. Terao, E. Lussetti, and F. Müller-Plathe, Phys. Rev. E **75** (5) (2007).

[7] E. Lussetti, T. Terao, and F. Müller-Plathe, J. Phys. Chem. B **111** (39), 11516 (2007).

[8] Y. Chatani, T. Inagaki, Y. Shimane, and H. Shikuma, Polymer **34** (23), 4841 (1993); Y. Chatani, Y. Shimane, Y. Inoue, T. Inagaki, T. Ishioka, T. Ijitsu, and T. Yukinari, Polymer **33** (3), 488 (1992); C. De Rosa, P. Rizzo, O. R. de Ballesteros, V. Petraccone, and G. Guerra, Polymer **40** (8), 2103 (1999).

[9] E. M. Woo, Y. S. Sun, and C. P. Yang, Prog. Polym. Sci. **26** (6), 945 (2001).

[10] F. Müller-Plathe, P. Bordat, M. Karttunen, I. Vattulainen, and A. Lukkarinen, Novel Methods in Soft Matter Simulations, Lecture Notes in Physics **640**, 310 (2004).

[11] C. De Rosa, G. Guerra, V. Petraccone, and B. Pirozzi, Macromolecules **30** (14), 4147 (1997).

[12] F. Müller-Plathe, Macromolecules **29** (13), 4782 (1996); R. Witt, L. Sturz, A. Dölle, and F. Müller-Plathe, J. Phys. Chem. A **104** (24), 5716 (2000); F. Müller-Plathe, Chem. Phys. Lett. **252** (5-6), 419 (1996).

[13] J. P. Ryckaert, G. Ciccotti, and H. J. C. Berendsen, J. Comput. Phys. **23** (3), 327 (1977); F. Müller-Plathe and D. Brown, Comput. Phys. Commun. **64** (1), 7 (1991).

[14] F. Müller-Plathe, Comput. Phys. Commun. **78** (1-2), 77 (1993); K. B. Tarmyshov and F. Müller-Plathe, J. Chem Inf. Model. **45** (6), 1943 (2005).

[15] H. J. C. Berendsen, J. P. M. Postma, W. F. van Gunsteren, A. Dinola, and J. R. Haak, J. Chem. Phys. **81** (8), 3684 (1984).

[16] C. De Rosa, G. Guerra, V. Petraccone, and P. Corradini, Polym. J. **23** (12), 1435 (1991).

[17] V. La Carrubba, S. Piccarolo, and V. Brucato, J. Polym. Sci. Pt. B-Polym. Phys **45** (19), 2688 (2007).

[18] G. Droval, J. F. Feller, P. Salagnac, and P. Glouannec, Polym. Adv. Technol. **17** (9-10), 732 (2006).

Chapter 4. Properties of polyvinyl alcohol oligomers: a molecular dynamics study

4.1.Introduction

Polyvinyl alcohol (PVA, ($H(-CH_2-CH(OH)-)_NCH_3$), where *N* is the number of repeat units, "monomers") is used in a large number of applications. Pervaporation membranes to remove residual water from organic solvents,[1] drug encapsulation and delivery,[2] the design of composite materials,[3] as well as metal nanoparticle stabilization[4] are just a few of them. A detailed knowledge of the physical properties of polymers as a function of the number of repeat units is the prerequisite for their optimum design in such applications. Physical key quantities are, e.g., the specific volume, the viscosity, geometrical parameters such as the radius of gyration as well as relaxation times which are relevant for process optimizations. In the past years simulations of the Molecular Dynamics (MD) type have become a powerful tool to evaluate such quantities in computer experiments. Nevertheless, such simulations are still a challenge for polymers with a large number N of repeat units. The long relaxation times for bond vectors require a prohibitive computational effort. It is thus necessary to perform model simulations on polymers with long chain length in order to estimate the accuracy and capability of MD approaches for these systems.

This is the focus of the present work in which have analyzed the static and dynamic properties of melts of PVA oligomers at a temperature T of 400 K. The data derived has not been considered in the literature up to now. By choosing T = 400 K we are above the measured glass transition of PVA at 358 K. In additional 300K simulations we have shown that the low-temperature MD results refer to PVA glass. For the simulations we have employed a force field that had been developed some time ago by one of the present authors for PVA as well as for different PVA solutions.[5] We have adopted those parameters without further modifications. The present contribution should be considered as one step to determine polymer lengths required to reproduce the

properties of real polymers. In this context we also have estimated the chain lengths in atomistic PVA melts that we required for reliable equilibration and sampling procedures to derive dynamic quantities.

4.2.Computational details

We have used the PVA force field of ref. 5 for the present MD simulations. The PVA data have been extracted from an ethanol force field by adding bond angle and dihedral angle terms that do not occur in the simple alcohol. As explained in detail in ref 5, ab initio and density functional calculations have been performed to optimize the force field parameters for the torsional behaviour. The capability of this setup has been documented in a number of publications.[5,6]

Table 4.1 summarizes some information on the simulated samples. Each system contains atactic PVA oligomers with methyl groups at both chain ends. The tacticity has been generated randomly for each of the chains. As shown already by Müller-Plathe and van Gunsteren[5] this method can be used to describe the formation of an atactic polymer by a free radical polymerization. Firstly, all samples except isopropanol have been prepared at 400 K (the measured glass temperature of PVA is 358 K[7]). The preparation has been carried out according to a procedure described by Milano and Müller-Plathe for polystyrene.[8] The conformation of each chain was generated separately using a hybrid pivot Monte Carlo molecular dynamics (PMC) approach,[9] as implemented in the GMQ software of Brown.[10] In PMC simulations, randomly picked dihedral angles are allowed to undergo a trial change. The method generates ensembles for a phantom chain, where two atoms interact with each other only if they are separated by less than a certain number of bonds. The bond cutoff, defining the boundary of the interatomic interactions, has been set to 7 as reported by Milano and Müller-Plathe.[8] The PMC method successfully generates melt-like conformations of apolar and polar polymer chains. The accuracy of the bond cutoff employed has not been quantified for the PVA polymers.

Despite differences in the interatomic interactions in the present work and ref. 8 we have chosen the same cutoff term. For each chain $2 \cdot 10^5$ pivot moves have been performed.

Table 4.1: Total number of chains, atoms and time windows t_s for the evaluation of quantities of the studied systems. Note that the. t_s number do not contain the time required for the relaxation.

System (repeat units per chain)	**Total number of chains**	**Total number Of atoms**	**t_s [ns]**
Isopropanol (=PVA monomer, *N*=1)	1250	15000	25
PVA oligomer (*N*=2)	800	15200	25
PVA oligomer (*N*=3)	600	15600	36
PVA oligomer (*N*=5)	400	16000	32
PVA oligomer (*N*=7)	300	16200	30
PVA oligomer (*N*=10)	200	15000	43 [a)]

a) Even after a relaxation of 45 ns followed by a simulation of 43 ns we observed a small slope [-8 J/(mol·ps)] in the total energy. Nevertheless, the 43 ns trajectory was used for the analysis.

We have placed the samples of isopropanol and longer chains into a separate periodic box at a reduced density of about 0.7 g/cm^3. The density of isopropanol at ambient conditions[7] amounts to 0.783 g/cm^3 and of amorphous PVA[11,12] up to 1.26

g/cm^3. For isopropanol we have carried out a simple relaxation at a constant temperature of 400 K and constant pressure of 101.3 kPa. The simulation has been terminated when the total energy and the mass density reached their equilibrium values. The systems were first energy-minimized to remove the most unfavorable contacts. Afterwards we have carried out a set of MD simulations of 200 ps each by using soft-core potentials as implemented in our simulation package YASP.[13] This allows the atoms to pass through each other and guarantees that the whole system gets rid of possible entanglements. Thus, the strain is minimized. We have performed eight relaxation simulations starting with the potential energy $V_0 = 0.3\ k_BT$ at zero atom-atom distance[13] and ending with $V_0 = 60\ k_BT$ before using the full non-bonded potential. The six intermediate V_0 parameters chosen amount to 1.5, 6, 12, 24, 36, 48 k_BT. This step was followed by a relaxation simulation of the oligomer bulk at a constant temperature of 400 K and a constant pressure of 101.3 kPa until the total energy and the mass density reached their equilibrium values. After this step, the production simulations have been carried out (Table 4.1).

All production simulations of isopropanol and the PVA bulk have been done under NPT conditions using the program YASP.[13] The temperature and pressure were kept constant using the Berendsen thermostat and barostat[14] with coupling times of 0.2 ps and 3.0 ps, respectively. The simulation time step was 2 fs with a sampling period of 2 ps. We have updated the neighbor list to calculate the nonbonded Lennard-Jones interactions every 15 time steps. A cutoff radius of 1.1 nm for the neighbor list and 1.0 for the potential has been chosen. To derive the electrostatic contribution we have used the reaction field method with a value of 19.92 for the dielectric constant (relative permittivity) of isopropanol.

4.3. Results and discussion

4.3.1. Density, specific volume and distribution of the atoms

Before discussing any properties of melts of PVA oligomers one should try to prove the validity of the model chosen. For this purpose, the density of the system was obtained also at a temperature of 300 K. All constant pressure (*NPT*) simulations were

first equilibrated with respect to the total energy and density of the system. The initial coordinates for the cooling to 300 K were taken from oligomer systems equilibrated at a temperature of 400 K. The calculated density of isopropanol (PVA oligomer N=1) was found to be 0.812±0.002 g/cm^3. This value is 3.7% larger than the experimental 298 K value of 0.7827 g/cm^3.[7] For the N=2 system 2,4-pentanediol we notice that the present MD result of 0.949 g/cm^3 is by only 1.5 and 0.6% smaller than the experimental value of 0.9635 and 0.955 g/cm^3.[15] Now let us consider the PVA system. Davidson[11] and Brandrup *et al*.[12] reported an experimental density of amorphous PVA at 298 K of 1.26 g/cm^3. The chains adopted in the present contribution are too short for a direct comparison with experiment. Thus the density of a simulated long-chain PVA ($1/N \sim 0$) can be only extrapolated. In Figure 4.1 such an estimate is displayed for the specific volume (i.e. inverse density) which is plotted as a function of the inverse number of "monomers" ($1/N$). A similar linear dependence as encountered in the diagram was found previously by Dollhopf *et al*. for *n*-alkanes.[16] We want to mention, that the extrapolated density of an infinite PVA chain as derived from the experimental values of isopropanol and 2,4-pentanediol is two times smaller than the one which is actually found.[11,12] Therefore only the specific volumes of PVA oligomer systems with a chain length of N=5,7,10 were used to estimate the PVA density in the limit $N \to \infty$ by a linear fit similar to the one in Figure 4.1. Despite the limitation to three data points the MD based extrapolated density of amorphous PVA with infinitely long chains of 1.182±0.003 g/cm^3 is only 6.2% lower than the experimental value. Note that the specific volume displayed in the figure leads to an extrapolated value larger than the experimental number. Our simulations indicate that smaller oligomers up to N=10 formula units per chain can be employed to estimate the density or the specific volume of very long PVA chains.

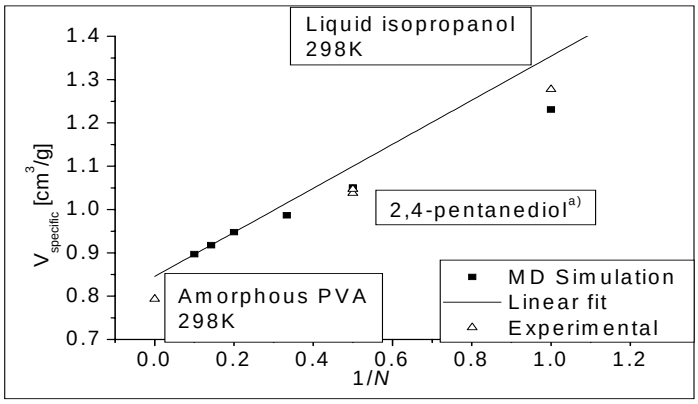

Figure 4.10: Specific volume of melts of PVA oligomers as a function of the inverse chain length at T=300 K. The value of amorphous PVA at 298 K[11,12] was put at $1/N = 0$. This choice is based on the assumption that the PVA chains reported in the literature[11] are longer than the ones simulated here. Note that the N=1, 2 systems have been omitted in the linear fit.

[a)] The data for 2,4-pentanediol is taken from the ChemExper catalog.[15]

Figure 4.2 shows the specific volume distribution of PVA melts at temperatures of 300 and 400 K as a function of $1/N$. It could be expected a priori, that the estimated high-temperature specific volume (density) is higher (lower) than the 300 K volume (density). In the limit $N \to \infty$ the density at 400 K amounts to 1.153±0.004 g/cm^3. In analogy to T=300 K, the density was estimated from the data points obtained for PVA melts of oligomers with chain lengths N=5,7,10. To the best knowledge of the authors, experimental data that could be compared with the present 400 K simulation, have not been reported up to now.

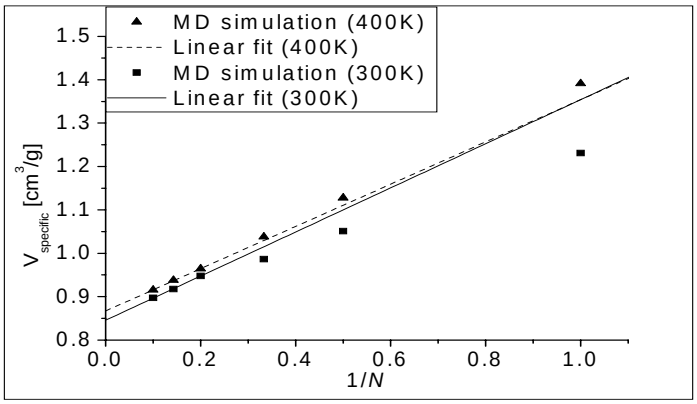

Figure 4.11: Specific volume of PVA oligomer melts as a function of the inverse chain length at T=300, 400 K. In analogy to Figure 4.1 the N=1 and 2 data have been omitted in the linear fit.

Figures 4.3 and 4.4 depict the radial distribution function (RDF) of the oxygen atoms and the neighboring methine carbons in PVA melts at 400 K. The structural details in the RDF indicate the liquid nature of isopropanol at this temperature. The comparison of the oxygen RDF for PVA oligomers with $N \geq 2$ shows that the major peak occurs approximately at the same position as in the case of the hydrogen bond of isopropanol (around 0.29 nm). From Figure 4.3a we deduce that the longer PVA chains form a melt with higher density. This leads to enhanced RDF peaks at slightly shorter distances. In Figure 4.3b we can identify the presence of weak additional peaks in systems with larger N which are of *intra*molecular origin.

For melts of PVA oligomers with a chain length $N \geq 2$ we see a set of peaks with reduced intensity between the two major ones (0.28 – 0.55 nm) that is absent in overheated, liquid isopropanol (N=1). The first major peak at 0.28 nm for $N \geq 2$ arises both from *intra*molecular and *inter*molecular hydrogen bonds between hydroxy groups. The *intra*molecular part is due to oxygen atoms from neighboring repeat units. The second prominent peak at 0.55 nm is created by *inter*molecular and *intra*molecular atoms far apart. All small peaks between the major ones are predominantly of *intra*molecular origin. They are an outcome of the equilibrium values of the bond lengths, angles and –

partially - torsions. These geometrical parameters prevent that *intra*molecular oxygens can occupy energetically preferable positions. For oligomers with chain length $N \geq 3$, one additional weak peak appears at 0.67 nm overlapping with the broad major peak at 0.55 nm. In isopropanol and pentane(2,4,)diol (N=2) the weak peak at 0.67 nm is absent. Both the 0.55 nm peak and the weak shoulder at 0.67 nm are of *intra*molecular origin. Their relative sharpness (see Figure 4.3a, N=2,3) also supports this assignment.

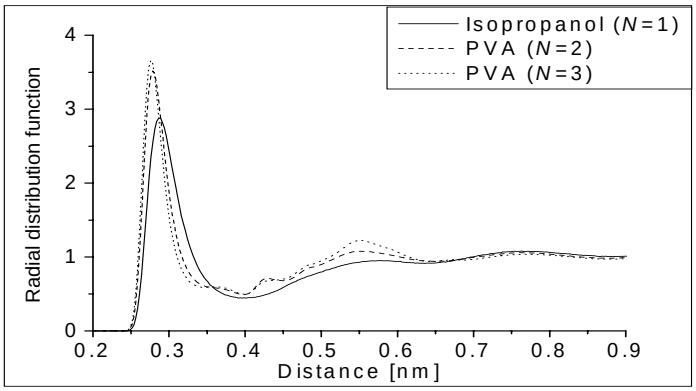

Figure 4.12a

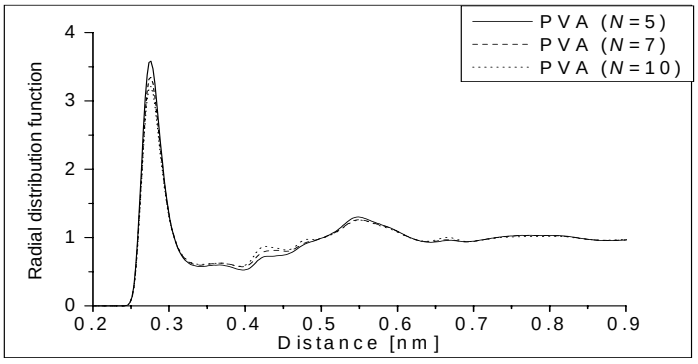

Figure 4.12b

Figure 4.12: Radial distribution function between oxygen atoms in melts of PVA oligomers with chain lengths N=1,2,3 (a) and N=5,7,10 (b) at 400 K.

The RDFs of the methane carbon atoms (Figure 4.4) carrying the hydroxyl groups are similar to the distribution of the hydroxyl oxygens. In Figure 4.4 it is possible to

correlate each peak in the C(CO)-C(CO) RDF to a characteristic peak in the O-O RDF. To a certain extent one can identify the fingerprints of the monomers in the RDF of the long-chain systems. There are a few interesting features that are completely absent for isopropanol (*N*=1) and partially absent for pentane(2,4)diol (*N*=2) (Figure 4a), but appear in the melts of longer PVA oligomers (Figure 4.4a and b). As the chain length increases and the mobility of the chains decreases, one can identify a set of small sharp peaks at 0.47, 0.52, 0.7, and 0.77 nm. In analogy to the oxygen RDF, these peaks are due to *intra*chain carbon pairs. They seem to be somewhat sharper than the corresponding peaks in the oxygen RDFs. This can be explained by the fact that the methine carbon atoms are linked through fewer bonds than the oxygen atoms.

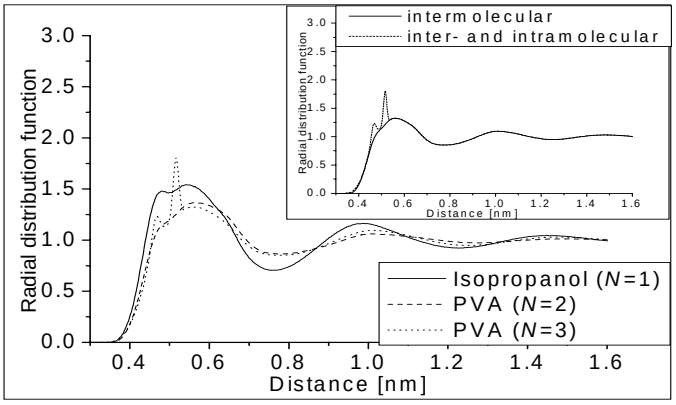

Figure 4.13a

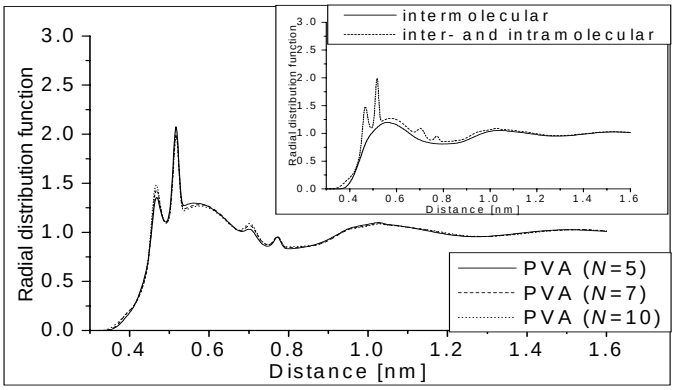

Figure 4.13b

Figure 4.13: Radial distribution function between methine carbon atoms (connected to oxygen) in melts of PVA oligomers with chain lengths *N*=1,2,3 (a) and *N*=5,7,10 (b) at 400 K. In the inserts we have fragmented the radial distribution function into intra- and intermolecular contributions. *N*=3 has been chosen in the first diagram, *N*=10 in the second one.

The calculated gyration radii of all PVA melts including isopropanol are shown in Figure 4.5. It was found that the gyration radius depends on the number of repeat units in the chain via the relation $R_{\text{gyration}} = N^{0.65\pm0.03}$. The calculated exponent is somewhat larger than the known N dependence for long chains in a good solvent ($R_{\text{gyration}} = N^{0.588}$).[17] In the melt, random walk statistics (~$N^{1/2}$) would be expected for infinite chains. The higher exponent in this work is probably owed to the shortness of the oligomers.

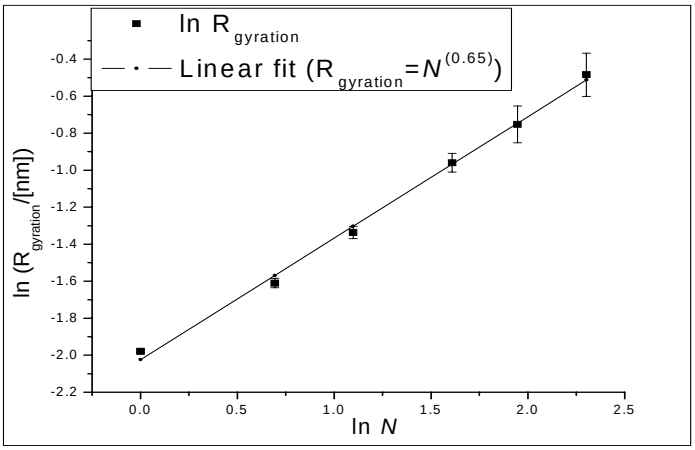

Figure 4.14: Double logarithmic representation of the gyration radius of PVA chains as a function of the chain length (the error bar is the standard deviation).

4.3.2. Relaxation and diffusion

Relaxation processes in PVA melts were studied via the orientation correlation function (OCF) $C_1(t) = \langle \cos(\varphi(t)) \rangle$ for the different bond vectors (O-H, O-C, C-C [internal] – all internal CH(OH)-CH_2 bonds only, C-C [end] – CH(OH)-CH_3 bonds at the

end of chains only) and chain end-to-end vectors (see Figures 4.6 and 4.7). The averaging in the OCFs covers all molecules in the simulation box. $\varphi(t)$ is the angle by which the vector rotates during the time interval *t*. The decay of the OCF for the O-H bond vector shows the behavior expected for the high viscosity of long PVA chains (Figure 4.6), i.e. their relaxation times are large. There is also a sizeable difference between melts of oligomers with the chain length $N \leq 3$ and $N \geq 5$. The OCF for the O-H bond vector in melts (liquids) of the shorter PVA oligomers decays within a time much smaller than 2 ns. In PVA chains with the length $N \geq 5$, the OCF decays much slower. For N=5 it takes more than 40 ns to approach zero. For the longer oligomers (N=7,10), these times are even longer.

In Figure 4.7 we compare the OCFs of different bond vectors and end-to-end vectors for N=3 and N=10. The OCF for other oligomers are not shown. For the oligomers with N=3 and shorter (Figure 4.6), all correlation functions reach zero in less than 4.7 ns. For PVA oligomers with N=10, on the other hand, none of the given OCF approaches zero even after 45 ns. While the OCF for all bond vectors exhibits - to a certain extend - decay properties, the OCF of the end-to-end vector is almost constant (Figure 4.7b) on the time scale of our simulations. The OCFs of the end-to-end vector for the other shorter oligomers with N=5 and 7 decay only slightly faster. We have to confess that simulations over much larger time windows would be necessary to derive quantitative information on the decay properties of the $C_1(t)$. Unfortunately such MD runs are beyond the capability of the present computer facilities. Nevertheless we feel that the comparison between the data of short and long chains is useful to indicate qualitative differences in the dynamic properties.

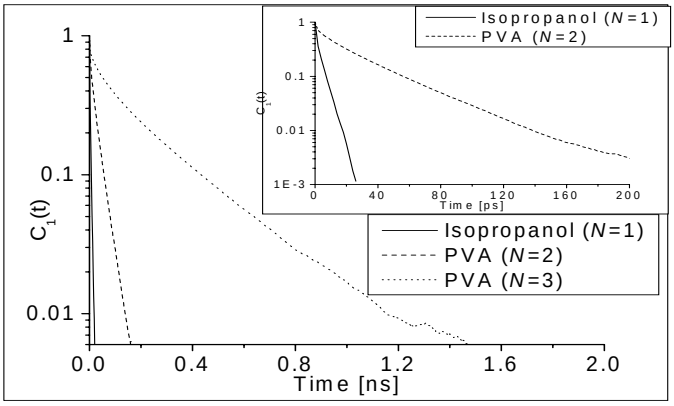

Figure 4.15a

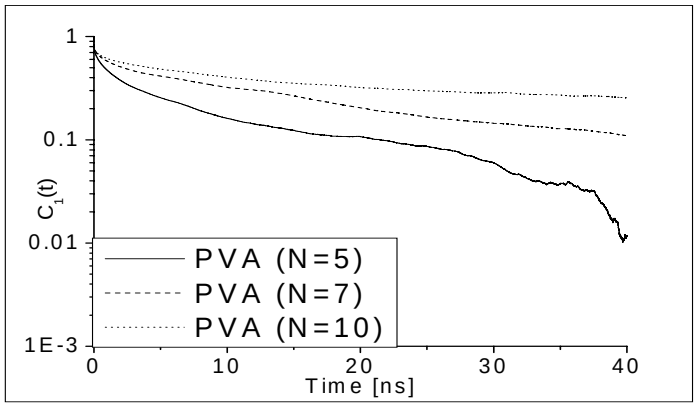

Figure 4.15b

Figure 4.15: Orientation correlation function of the O-H bond vector for melts of PVA oligomers with the chain length *N*=1,2,3 (a) and *N*=5,7,10 (b) at 400 K. The insert in figure (a) shows the orientation correlation functions for isopropanol (*N*=1) and 2,4-pentanediol (*N*=2) at higher resolution. Note the logarithmic scale for the y-axis.

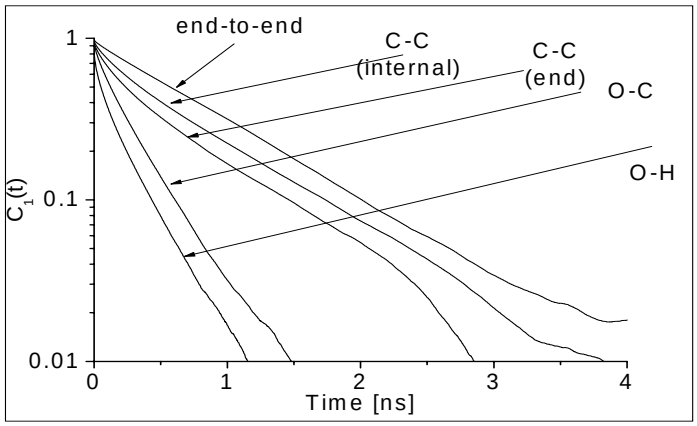

Figure 4.16a

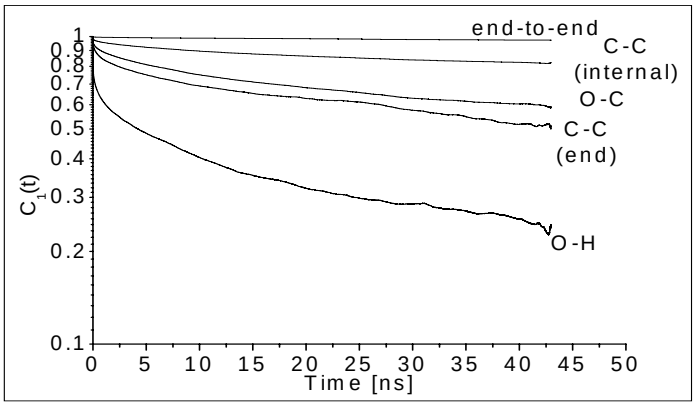

Figure 4.16b

Figure 4.16: Orientation correlation function for the bond vectors (O-H, O-C, CH-CH_2 [internal], CH-CH_3 [end]) and the end-to-end vectors for melts of PVA oligomers with the chain length N=3 (a) and N=10 (b) at 400 K. In analogy to Figure 4.6 a logarithmic y-axis scaling has been employed.

An attempt was made to fit the OCFs to the Kohlrausch-Williams-Watts (KWW) expression $\exp\left(-\left[t/\tau\right]^{\beta}\right)$. The values for the relaxation time τ and the stretching parameter β were then used to calculate the average relaxation time $\langle\tau\rangle = (\tau/\beta)\,\Gamma(1/\beta)$, where Γ is the gamma function. As a reasonable fit of all OCFs to the KWW formula has been impossible, only some of the relaxation times could be determined. The calculated $\langle\tau\rangle$ values are plotted in Figure 4.8. All relaxation times in the $N\leq 3$ family depend

exponentially on the number of monomers. A reasonable fit for the bond vector C-C [internal] and the end-to-end vector of PVA chains for N=5,7, and 10 was possible only for the O-H (N=5,7,10), O-C (N=5,7), and C-C [end] (N=5) bond vectors. In the melt of PVA oligomers with N=5 the O-H, O-C, and C-C [end] bond vectors reproduce relaxation times already found in the first group of PVA melts (N=1,2,3). For the PVA oligomers with N=7,10, an exponential increase cannot be confirmed yet. Such a dependence, however, cannot be excluded completely as full relaxations of PVA melts probably have not been reached (cf. Table 4.1, Figure 4.6b and 4.7b). Larger trajectories are required for these melts to render a quantitative analysis possible.

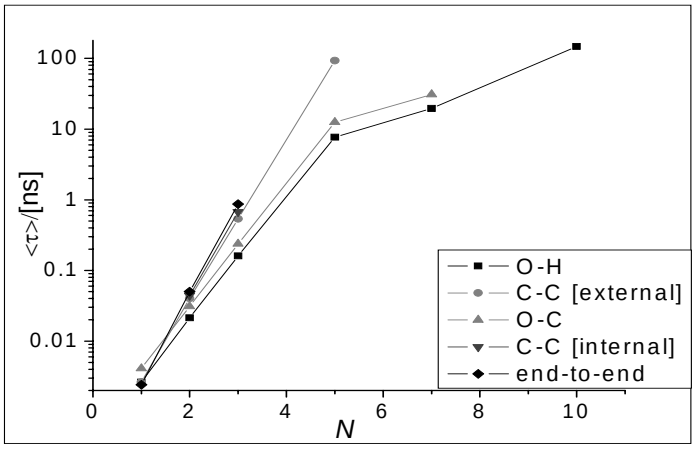

Figure 4.17: Average relaxation times $\langle\tau\rangle$ obtained by fitting the orientation correlation function for different bond vectors and the end-to-end vector of PVA oligomers to the Kohlrausch-Williams-Watts expression. We have chosen an exponential ordinate scaling to observe a linear behavior in connection with the KWW formula. Data points are only given for systems where it has been possible to obtain a reasonable fit.

In the present work the self-diffusion of oxygen, C [internal] (CH_2 and CHOH), and C [end] (terminating CH_3) atoms was studied, too. The calculated self-diffusion coefficients are given in Table 4.2. As could be expected (see also the decay of the OCFs), the diffusivity of the atoms in a melt decreases with increasing chain length. It is

worth mentioning that diffusion coefficients of the chains with *N*=7-10 are extremely small (upper bound ≈ $1 \cdot 10^{-9}$ cm^2/s). But note that similar numbers have been found in an experimental NMR study of PVA in water solution.[18] The simulation times accessible restrict the determination of the center-of-mass diffusion coefficients of PVA oligomers to the *N*=1,2 and *N*=3 (not shown) species.

In analogy to the work of Bennemann *et al.* we have shown in Figure 4.9 the mean square displacement (MSD) of the oxygen atoms for different PVA melts in a double logarithmic scale.[19] The MSD in the melt of the *N*=3 system reflects quite fast diffusion of oxygen during the first few picoseconds; later it becomes a little slower. For the longer PVA chains (*N*=5,7,10) this effect is more pronounced. It can be explained by differences in the diffusion modes. At short times up to 0.5 ns, we have "free" diffusion. After this time the connection of the atoms to the chain slows down their diffusion. This mechanism is well known for polymer melts.[20] The diffusion of the other atoms is similar to the behavior of oxygen. At least in the time interval considered, the simulations do not reproduce details of the Rouse model.[20] Probably the chains considered are still too short. As discovered by Ding *et al*., oligomer chains establish a polymer-like behavior consistent with the Rouse dynamics for molecular weights exceeding the "monomer" weight by a factor larger than 20.[21]

Table 4.2: The self-diffusion coefficient of different atoms in melts of PVA oligomers with different chain lengths.

System (chain length)	**Diffusion coefficient [cm^2/s]**			
	O (OH)	**C (CH_3)**	**C (CH_2 and CHOH)**	**Center of mass**
Isopropanol (PVA oligomer *N*=1)	$3.4 \pm 0.2 \cdot 10^{-5}$	$3.4 \pm 0.2 \cdot 10^{-5}$	$3.4 \pm 0.2 \cdot 10^{-5}$	$3.4 \pm 0.2 \cdot 10^{-5}$
PVA oligomer (*N*=2)	$4.8 \pm 0.2 \cdot 10^{-6}$	$4.8 \pm 0.2 \cdot 10^{-6}$	$4.8 \pm 0.2 \cdot 10^{-6}$	$5 \pm 3 \cdot 10^{-6}$
PVA oligomer	$5.9 \pm 0.1 \cdot 10^{-7}$	$6.2 \pm 0.2 \cdot 10^{-7}$	$5.9 \pm 0.2 \cdot 10^{-7}$	$5.3 \pm 2 \cdot 10^{-7}$

(*N*=3)				
PVA oligomer (*N*=5)	$1.2\pm0.1\cdot10^{-8}$	$2.04\pm0.03\cdot10^{-8}$	$1.37\pm0.04\cdot10^{-8}$	-
PVA oligomer (*N*=7)	$5.9\pm0.3\cdot10^{-9}$	$1.5\pm0.1\cdot10^{-8}$	$7.37\pm0.4\cdot10^{-9}$	-
PVA oligomer (*N*=10)	$2.0\pm0.1\cdot10^{-9}$	$1.9\pm0.1\cdot10^{-9}$	$1.1\pm0.1\cdot10^{-9}$	-

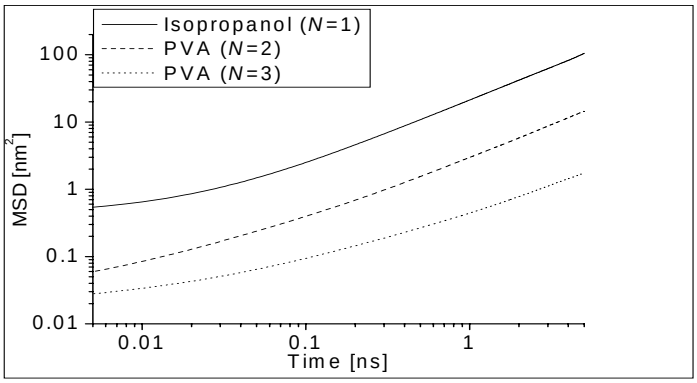

Figure 4.18a

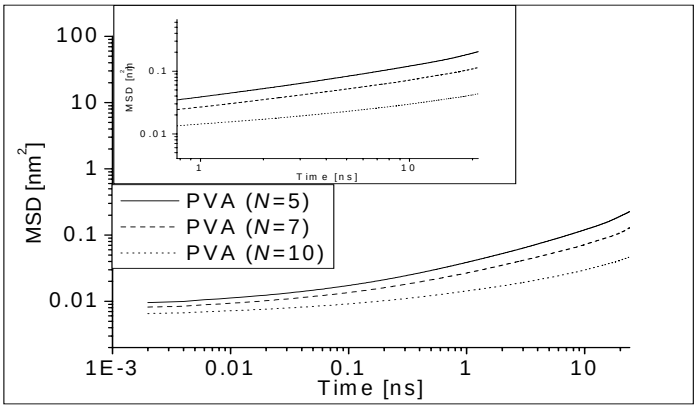

Figure 4.18b

Figure 4.18: Mean square displacement of the oxygen atoms in melts of PVA oligomers with *N*=1, 2, 3 (a) and *N*= 5, 7, 10 (b) at 400 K in a double logarithmic representation.

The insert in figure (b) shows the mean square displacement in the melt of the *N*=5,7,10 materials in an enhanced scale.

4.4. Summary

Properties of melts of polyvinyl alcohol oligomers with different chain lengths (*N*=1,2,3,5,7,10) were studied at 300 and 400 K. Isopropanol (*N*=1) at 400 K has to be regarded as an overheated liquid. The specific volume of the polymers studied depends reciprocally on the number of repeat units. Such a behavior has been found previously by Dollhopf *et al*. for *n*-alkanes.[16] Modifications of the radial distribution function of oxygen and carbon as a function of the polymer length follow expectations: the peaks become more pronounced for longer PVA oligomers. Here the molecules are less mobile and the melt becomes more viscous. Both *intra*chain and *inter*chain contributions to the RDF peaks have been assigned. The gyration radius depends on the number of formula units via $R_{gyration} = N^{0.65\pm0.03}$.

For dynamical information, orientation correlation functions were studied. It was found that all bond and end-to-end vectors of PVA oligomers with *N*=1,2,3 relax completely within a few nanoseconds. For longer PVA oligomers, the relaxation takes much more time. Whenever possible, the Kohlrausch-Williams-Watts expression was used to fit and integrate the OCFs to obtain the relaxation times. The relaxation time for O-H, O-C, and C-C [end] scales exponentially with the chain length up to *N*=5. For longer oligomers, the dependence is not clear. This might be due to insufficient simulation times for PVA oligomers with *N*=7 and 10, or due to the onset of a different scaling behavior for longer chains.

The mean square displacement of the hydroxyl oxygens and backbone carbon atoms in all PVA melts has been calculated. The short PVA oligomers (*N*=1,2) are closer to a liquid-like behavior. The MSD increases linearly from the start. PVA oligomers with *N*=3 are an intermediate case. For the PVA oligomers with *N*=5,7 and 10 the diffusion of the atoms within the first pico- or nanoseconds is faster (so-called “free diffusion”). After

this period the atoms “feel” the constraints of the chain and the overall diffusion slows down so that anomalous diffusion is found. Quantitative agreement of the present findings with the Rouse model has not been observed.[20] It seems that the oligomer chains considered are still too short to reproduce a polymer-like behavior compatible with this approach,[21] although the simulations have reached the present computational limits.

From the dynamic properties of PVA melts with shorter oligomers (i.e. *N* up to 10) one can conclude that the simulation of a melt of longer PVA chains on a full atomistic level is currently not feasible. In simulations of interfaces between PVA meltsand solid (metallic) surfaces this becomes even more evident. Larger systems are required for a proper modelling. The relaxation times at the interface are also much longer than in the bulk.[22] Therefore, coarse grained simulations of PVA melts[23] seem to be the method of choice to study the behaviour of PVA near a solid surface.

4.5. References

[1] B. X. Cai, J. Appl. Polym. Sci. **101** (2), 1160 (2006).

[2] G. Zuccari, R. Carosio, A. Fini, P. G. Montaldo, and I. Orienti, J. Control. Release **103** (2), 369 (2005); I. Orienti, A. Di Pietra, B. Luppi, and V. Zecchi, Arch. Pharm. Pharm. Med. Chem. **333**, 421 (2000); M. D. Kurkuri and T. M. Aminabhavi, J. Control. Release **96** (1), 9 (2004).

[3] H. S. Mansur and H. S. Costa, Chem. Eng. J. **137** (1), 72 (2008).

[4] A. N. Shipway, E. Katz, and I. Willner, ChemPhysChem **1** (1), 18 (2000); N. Toshima and T. Yonezawa, New J. Chem. **22** (11), 1179 (1998); H. Hirai, Y. Nakao, and N. Toshima, Chem. Lett. (9), 905 (1976); H. Hirai, Y. Nakao, and N. Toshima, Chem. Lett. (5), 545 (1978); P. Lu, T. Teranishi, K. Asakura, M. Miyake, and N. Toshima, J. Phys. Chem. B **103** (44), 9673 (1999).

[5] F. Müller-Plathe and W. F. van Gunsteren, Polymer **38** (9), 2259 (1997).

[6] K. B. Tarmyshov and F. Müller-Plathe, J. Chem. Phys. **126** (8), 74702 (2007); F. Müller-Plathe, J. Membr. Sci. **141** (2), 147 (1998); F. Müller-Plathe, J. Chem. Phys. **108** (19), 8252 (1998).

[7] *Handbook of Chemistry and Physics*, edited by D. R. Lide (CRC Press, Boca Raton, 1993-1994).

[8] G. Milano and F. Müller-Plathe, J. Phys. Chem. B **109** (39), 18609 (2005).

[9] S. Neyertz and D. Brown, J. Chem. Phys. **115** (2), 708 (2001).

[10] D. Brown.

[11] R. L. Davidson, *Handbook of water-soluble gums and resins*. (MacGraw-Hill, New York, 1980).

[12] *Polymer Handbook*, edited by J. Brandrup, E. H. Immergut, and E. A. Grulke (John Wiley & Sons, Inc., New York, 1999).

[13] F. Müller-Plathe, Comput. Phys. Commun. **61** (3), 285 (1990); F. Müller-Plathe, Comput. Phys. Commun. **78** (1-2), 77 (1993); K. B. Tarmyshov and F. Müller-Plathe, J. Chem Inf. Model. **45** (6), 1943 (2005).

[14] H. J. C. Berendsen, J. P. M. Postma, W. F. van Gunsteren, A. Dinola, and J. R. Haak, J. Chem. Phys. **81** (8), 3684 (1984).

[15]

[16] W. Dollhopf, H. P. Grossmann, and U. Leute, Colloid Polym. Sci. **259** (2), 267 (1981).

[17] J. des Cloiseaux and G. Jannink, Polymer in Solution; Their Modelling and Structure **Clarendon, Oxford** (1990).

[18] Y. E. Shapiro, J. Colloid Interface Sci. **212** (2), 453 (1999).

[19] C. Bennemann, J. Baschnagel, W. Paul, and K. Binder, Computational and Theoretical Polymer Science **9** (3-4), 217 (1999).

[20] K. R. Haire, T. J. Carver, and A. H. Windle, Comput. Theor. Polym. Sci. **11** (1), 17 (2001).

[21] Y. F. Ding, A. Kisliuk, and A. P. Sokolov, Macromolecules **37** (1), 161 (2004).

[22] K. B. Tarmyshov and F. Müller-Plathe, Soft Materials **5** (2&3), 135 (2007); C. F. Abrams, L. Delle Site, and K. Kremer, Phys. Rev. E **67** (2) (2003).

[23] D. Reith, H. Meyer, and F. Müller-Plathe, Macromolecules **34** (7), 2335 (2001).

Chapter 5: Study of the Soret effect in hydrocarbone chains / aromatic compound mixtures.

5.1. Introduction

In a binary mixture exposed to a temperature gradient, the Soret effect induces a concentration gradient.

$$\nabla x = -S_T x(1-x)\nabla T \qquad 5.1$$

where ∇x is concentration gradient, ∇T is temperature gradient and S_T is the Soret coefficient. $S_T = D_T / D$ is the ratio of the thermal diffusion coefficient and the collective diffusion coefficient. A positive Soret coefficient of the component with the mole fraction *x* implies that this component moves to the cold region of the fluid.

Although the discovery of the effect by Ludwig took place more than 150 years ago, there is so far only a limited microscopic understanding for liquids.[1] Apparently, the magnitude as well as the sign of S_T are very sensitive to the chosen mixture. Generally, there is no Soret effect in the mixture of absolutely equal components due to the principle of symmetry. The Soret effect is basically the response of the system to the difference between two mixing partners. This simple conception was investigated in detail by experiments and by simulations.

Molecular dynamics simulations of equimolar mixtures of particles[2] and spherical molecules[3] show that the component with the larger mass, the smaller radius and the larger depth of the interaction potential moves to the cold side. In the previous publication[4] have been shown experimentally and by reverse non-equilibrium molecular dynamic simulation (RNEMD) that the binary mixtures of simple molecules (tetraethylsilane, di-tert-butylsilane and carbon tetrabromide in carbon tetrachloride) obey this rule of thumb.

Another large group of substance studied are the hydrocarbons which have been investigated experimentally and theoretically[5-7]. However, for alkane/benzene mixtures[7] the simple rule of thumb fails. The heavier linear alkane always moves to the warm side. This tendency becomes weaker with increasing degree of branching and the highly

branched isomer of heptane (2,2,3 - trimethybutane) moves to the cold side and then benzene to the warm side. The trend that linear alkanes have the strongest tendency to move to the warm side had already be observed by Kramers and Broeder for n-nonane and n-hexadecane[5] compared to other hydrocarbons, such as the branched isooctane and one and two ring compounds.

The thermal diffusion behavior of linear alkanes is well described by a simple lattice model (SLM)[7]. At the same time the SLM is not capable to describe the thermal diffusion behavior of branched alkanes because their thermodynamic parameters such as density, heat capacity and thermal expansion coefficient are not sensitive to the degree of branching. Recently, the influence of the degree of branching by RNEMD simulation has been investigated.[8] The simulated Soret and mutual diffusion coefficients reproduce the experimental trend. However, the simulated values of S_T values are systematically $\approx 3 \cdot 10^{-3} K^{-1}$ lower than in the experiment. The observed decrease of the magnitude of S_T for equimolar alkane/benzene mixtures with branching of the alkane can not be explained by mass and size effects. The effect of the molecular shape, which affects the liquid structure, as well as kinetic properties of the mixture, needs to be considered additionally. However, has not been found a simple relation to take branching or, more generally, molecular shape, into account.

In this research we extend the work by considering hydrocarbon chain /aromatic compound mixtures. Benzene was replaced by cyclohexane and two xylene isomers (p-xylene and o-xylene). As a solute we used heptane, two of its isomers 2,3-dimethylpentane (2,3-DMP) and 2,4- dimethylpentane (2,4-DMP). Experiments were performed using the thermal diffusion forced Rayleigh scattering technique. The experimental results were compared with RNEMD simulations. Additionally, we investigated the effect of intramolecular flexibility using RNEMD by introducing two double bonds for 2,3-DMP and 2,4-DMP e.g. considering two alkenes: 2-methyl-3-methylenepent-1-ene (2,3-DMPEN) and 2,4-dimethylpenta-1,3-diene (2,4- DMPEN), respectively.

5.2 Experimental details

5.2.1 Sample preparation

Heptane, o-xylene (98%) and p-xylene (98%) were purchased from Fluka; 2,3-dimethylpentane (99%) and 2,4-dimethylpentane (99%) were ordered from Aldrich; cyclohexane (99.9%) we got from LiChrosolv. Figure 5.1 shows the chemical structure of the investigated molecules. For all mixtures the alkane mole fraction was adjusted by weighing the components. The TDFRS experiments require a small amount of dye in the sample. In this work, all samples contained approximately 0.002 wt% of the dye Quinizarin (Aldrich). This amount ensures a sufficient optical modulation of the grating but is small enough to avoid convection and contributions of the dye to the concentration signal. Before each TDFRS experiment, approximately 2 ml of the freshly prepared solution were filtered through 0.2 μm filter (hydrophobic PTFE) into an optical quartz cell with 0.2 mm optical path length (Helma) which was carefully cleaned from dust particles before usage.

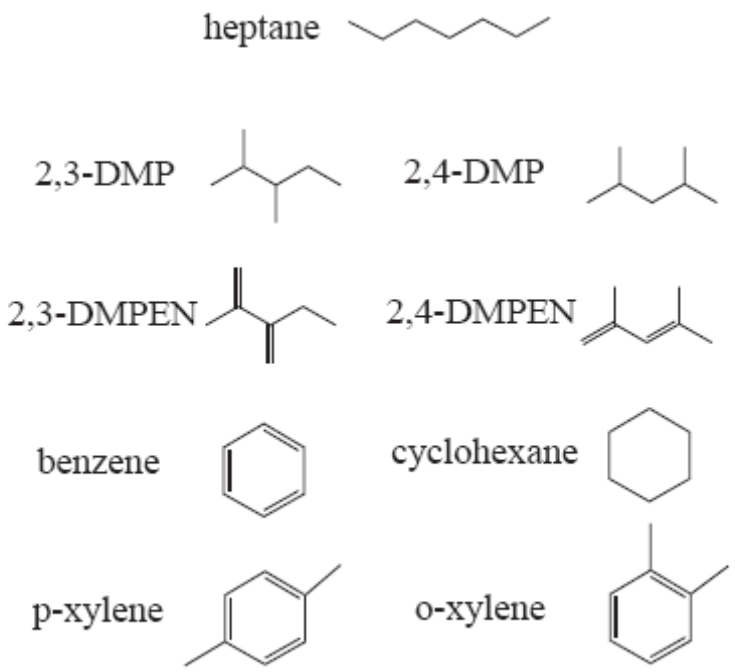

Figure 5.1: Chemical structure of the investigated molecules. The branched alkanes (or alkenes) are: 2,3-DMP (2,3-dimethylpentane), 2,4-DMP (2,4-dimethylpentane), 2,3-DMPEN (2-methyl-3- methylenepent-1-ene) and 2,4-DMPEN (2,4-dimethylpenta-1,3-diene).

5.2.2. Refractive index increment measurements

In order to determine the changes of the refractive index n with composition x at constant pressure P and temperature T, $(\partial n/\partial x)_{P,T}$ for each hydrocarbon chain/aromatic ring compound we measured the refractive index of several mixtures of different concentration around the equimolar mixture with an Anton Paar RXA 156 refractometer. The slope $(\partial n/\partial t)_{P,T}$ was then determined by linear interpolation. The temperature derivatives at constant pressure and composition, $(\partial n/\partial T)_{P,x}$, were determined from measurements with a Michelson interferometer(ref) in a temperature range of 3 C above and below the temperature of the thermal diffusion forced Rayleigh scattering TDFRS experiment.

5.2.3 TDFRS experiment and data analysis

In our thermal diffusion forced Rayleigh scattering (TDFRS) experiments, the beam of an argon-ion laser (λ_ω=488 nm) is split into two writing beams of equal intensity which interfere in the sample cell (ref) for a detailed description of the method). A small amount of dye is present in the sample and converts the intensity grating into a temperature grating, which in turn causes a concentration grating by the effect of thermal diffusion. Both gratings contribute to a combined refractive index grating, which is read out by Bragg diffraction of a third laser beam (λ_r=633 nm). The intensity $\zeta_{net}(t)$ of the signal depends on the transport coefficients and the index of refraction increments and may be expressed as

$$\zeta_{net}(t) = 1 + \frac{(\partial n/\partial x)_{P,T}}{(\partial n/\partial T)_{P,x}} S_T x(1-x)(1-e^{-q^2 Dt}) \qquad 5.2$$

where q is the grating vector, whose absolute value is determined by the angle _ between two writing beams and the wavelength λ_ω:

$$q = \frac{4\pi}{\lambda_\omega} \sin\frac{\theta}{2} \qquad 5.3$$

For the determination of the transport coefficients, is fitted to the measured heterodyne signal using the independently measured contrast factors $(\partial n/\partial t)_{P,T}$ and $(\partial n/\partial T)_{P,x}$

5.3. Computational Details

The Reverse Non-equilibrium Molecular Dynamics (RNEMD)[9] method has been applied to investigate the thermal diffusion of binary mixtures of alkane(alkene) in p-xylene o-xylene and cyclohexane. Lorentz-Berthelot mixing rules were employed for unlike non-bonded interactions. The force field parameters for the benzene ring of xylene were taken from Milano and Müller-Plathe.[10] The C-H bonds were slightly polarized in order to reproduce the quadrupole moment. For carbon and hydrogen of the methyl group of xylene we used the following Lennard-Jones parameters: ε = 0.22/0.15 kJ/mol and σ = 0.3/0.245 nm, respectively.

For alkanes, alkenes and cyclohexane we used the TraPPE-UA[11,12] force field. All CH_n groups were treated as individual atoms without taking into account electrostatic

interactions. We would briefly like to mention the differences between the force fields for alkanes and alkenes. For the CH_2 and CH_3 groups present in both alkane and alkene, we used the same Lennard-Jones parameters. We took into account the difference in shape due to the double bond by appropriate new LJ parameters of sp^2 geometry,[12] angle, and bond length changes, which lead to the expected different specific volume for alkene compared to alkane. Only constrained bonds were used in the simulation, which were kept rigid by the SHAKE algorithm.[13] For the electrostatic interactions, the reaction field method has been used with a dielectric constant of 2.06 which is the average value of the alkanes and the xylenes. We found a good agreement between simulated and experimental values for the density, heat of vaporization and self diffusion of the xylene molecules (c.f. Table 5.1). Unfortunately, we could not find any reliable experimental values for the self diffusion coefficient of o-xylene but it is in the same order of magnitude as for benzene molecule.[10]

All simulations were performed by the program YASP[14] with periodic boundary conditions in all directions for as least 12 ns. The time step was 2 fs. The non-bonded cutoff was 1.2 nm for the neighbour list and 1.1 nm for the interactions. The neighbour list was updated every 15 time steps. The temperature and pressure were kept at 298 K and 101.3 kPa using the Berendsen method with a coupling times of 0.2 ps for the temperature and 5 ps for the pressure.[15] For every system is consisted 320 molecules, equilibrium was performed for at least 4 ns. After this period, the fluctuations of the total energy and density over 500 ps were in all cases below 2%.

Table 5.1: The comparison of the physical properties of xylene obtained from the simulation and experimental work.

	p-xylene		o-xylene	
	experiment	Simulation	experiment	Simulation
$density(\rho / gm \cdot L^{-1})$	0.86[16]	0.858 ± 0.002	0.86[16]	0.864 ± 0.003
$heat\_of\_vaporization$ $(H_{vap} / kJ \cdot mol^{-1})$	42.38[17]	41.7 ± 0.1	43.43[17]	37.5 ± 0.1

$self-diffusion\_coefficient$ $(D/10^{-5} cm^2 s^{-1})$	4.1^{18}	2.24 ± 0.2	-	1.78 ± 0.2

For Soret coefficient calculation every cell of mixture was replicated three times in the direction of temperature gradient (in our case is z direction, means Lx=Ly=Lz/3= 4-4.2nm). All RNEMD simulations were performed at constant NVT conditions. The periodic system was divided into 20 slabs. The average temperature was kept at 298 K. The temperature gradient was created by exchanging every 100th (N_{100}) step the center of mass velocity vector of two molecules (”coldest” molecule in the hot slab one and the ”hottest” molecule in the cold slab eleven) of the same type. The temperature profile were sampled every 101th step. After the concentration gradient is induced the Soret coefficient can be calculated. For each simulation run two values of the Soret coefficient were calculated: from the nine slabs of the downward branch and from the nine slabs in the upward branch. The hottest and coldest slabs have been excluded from the analysis. The final value of S_T represents the average value, the error bars reflect the difference between S_T from downward and upward branches.

5.4. Results and Discussion

5.4.1. Experiment

Figure 5.2 shows the experimentally determined Soret coefficient for different hydrocarbon/ aromatic compound mixtures. For all considered solvents the magnitude of S_T becomes smaller with increasing degree of branching of the first component and is also sensitive to the nature of the second component. This is the same trend which we observed for other heptane isomers in benzene.[7] It is remarkable, that all curves have the same shape and no intersection points were observed.

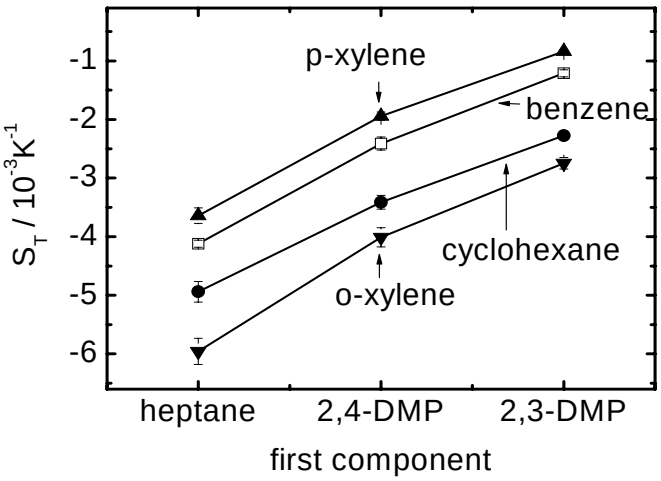

Figure 5.2: The experimentally measured Soret coefficients for equimolar mixtures of some alkanes and alkenes in different aromatic compounds. The data for hydrocarbon/benzene mixtures were taken from Polyakov et. al.[8]

The obtained results can be analyzed within a phenomenological conception proposed by Wittko in his PhD dissertation.[19] They assumed that the Soret coefficient for a given mixture (of the component A in the component C) is only determined by the difference in the properties of the pure mixing partners σ^A and σ^C, respectively

$$S_T^{AC} = \sigma^A - \sigma^C \qquad 5.4$$

σ might be interpreted as heat affinity. Thus, the Soret coefficient of the components A in the component C (S_T^{AC}) can be calculated using S_T^{AB} and S_T^{CB}:

$$S_T^{AC} = S_T^{AB} - S_T^{CB} \qquad 5.5$$

Figure 5.3 shows a satisfactory agreement between the experimental values of the Soret coefficient S_T and the calculated S_T^{calc} using Eq. 5.4.

In order to determine the heat affinities an overestimated linear equation of the form

$$M\vec{\sigma} = \overrightarrow{S_T} \qquad 5.6$$

has to be solved. $\vec{\sigma}$_ and $\overrightarrow{S_T}$ are vectors consisting of the heat affinities and Soret coefficients of the different solvents and M is a Matrix consisting of 1, -1 and 0

combining the corresponding solvents with their Soret coefficients and heat affinities. In order to determine the heat affinities we have to rewrite the equation system.

$$\vec{\sigma} = (M^T M)^{-1} M^T \overrightarrow{S_T} \qquad 5.7$$

The heat affinities are only determined up to an arbitrary constant, which we have chosen to be zero for o-xylene, the substance with the lowest tendency to move to the warm side. The substance with the largest affinity to the cold is the asymmetric heptane. The calculated Soret coefficients are perfectly described by a straight line through the origin with a slope of 0.99±0.03.

Our series of heat affinities shows parallels with the logarithm of the separation factor S given by Kramers and Broeders[5]. Also they found the lowest values for ”log S” for the two linear alkanes n-nonane and n-hexadecane followed by the branched iso-octane, one ring compounds (xylene, ethylcyclohexane, p-cymene) and two ring compounds (isopropyl-napthalene, α -methylnaphtalene).

Table 5.2: Physical properties for the solvents used in the analysis by Eq. 5.8: heat of vaporizationat the boiling point[20,21], density at room temperature[20] and the principal moment of inertia.[22]

solvent	ΔH_{vap} / kJ/mol	ρ / g·cm^{-3}	Ixx Å^2	Iyy Å^2	Izz Å^2
heptane	36.57	0.684	44	661	681
2,4-DMP	33.1	0.673	123	349	425
2,3-DMP	34.1	0.695	149	269	292
benzene	33.83	0.874	82	821	164
cyclohexane	33	0.774	117	117	203
p-xylene	42.38	0.857	89	328	410
o-xylene	43.43	0.876	149	220	362

The importance of the molecular shape for the thermal diffusion in binary mixtures of two disk-like molecules was recently investigated for a mixture of benzene and cyclohexane by Debuschewitz and Köhler.[23] They correlated the Soret coefficient with the difference in mass and in the component of the moment of inertia perpendicular to the molecular plane. In our case we have difficulties with the quantitative application of this conception because it is not clear which component of the moment of inertia needs to be considered for the alkane molecules. At the same time, it is clear that the observed "parallel shift" of the curves (c.f. Figure 5.2) with the substitution of the solvent (benzene, cyclohexane, p- or o-xylene) is related to the physical properties (difference in mass and moment of inertia) of these cyclic components. As a simple approach, we related the heat affinity with the product of heat of vaporization ΔH_{vap} and the density ρ (or in other words this product equal to cohesive energy density), the mass and the ratio of the largest to the smallest moment of inertia.

$$\sigma = \gamma \cdot \Delta H_{vap} \cdot \rho + \alpha \cdot m + \beta \cdot I^{\max} / I^{\min} \qquad 5.8$$

where γ, α, β are constants. The first term should account for the chemical contribution, the second term for the mass and the last term for the asymmetry of the molecule. The expression of the chemical contribution will certainly break down in the case of polar substances[19], but it might also loose its validity, if one considers other systems than alkanes. Also, the contribution of the asymmetry becomes difficult in the case of larger and more flexible molecules.

The black round symbols in the lower right part in Figure 5.3 show the correlation of σ and σ^{calc} according to Eq. 5.8 with $\gamma = 1.74 \times 10^{-4}\ mol\ cm^3/(kJ\ g\ K)$, $\alpha = -6.57 \times 10^{-5}\ mol/(g\ K)$ and $\beta = -2.38 \times 10^{-4}\ K^{-1}$. The straight line corresponds to a line fit with a slope of 0.88 and an intercept of 2.74×10^{-4}. The correlation coefficient is only in the order of 0.93. Considering the component of moment of inertia perpendicular to the molecular plane I_{zz} leads to slightly lower correlation coefficient of 0.89. Especially the correlation for the organic ring compounds degrades, while the correlation of the alkanes slightly improves. Additionally, we can replace the chemical contribution

by $\sqrt{H_{vap}\rho}$, which corresponds to the Hildebrandt parameter δ. This decreases the correlation coefficient further to 0.81.

Finally, we would like to point out that we did not consider excess effects in Eq. 5.4 and 5.8, which play an important role in the thermal diffusion behavior of liquid mixtures.[24] Due to the limited number of equimolar mixtures studied we were also not able to account for a change in composition. Whether this simple approach according to Eq. 5.8 holds also for other nonpolar systems needs to be investigated in the future for a large number of systems.

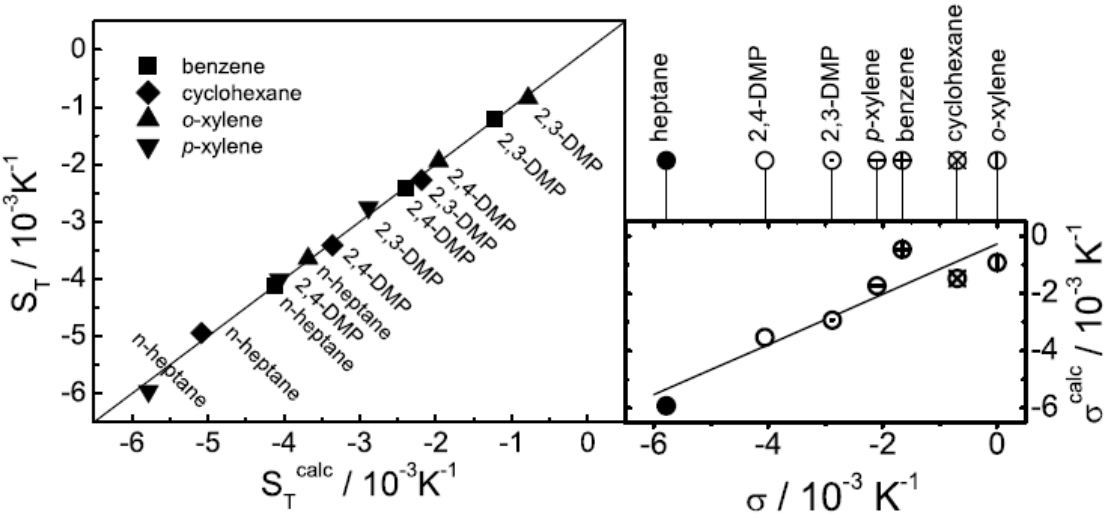

Figure 5.3: The comparison of the experimental values of the Soret coefficient and the predicted ones using Eq. 5.5. The upper right part of the figure shows the heat affinity σ of each solvent, which have been used to calculated S_T^{cal} . In the lower right part of the figure σ is correlated with the calculated heat affinity σ^{cal} calc according to Eq.5.6 (black round symbols).

5.3.2.. Simulation

Additionally, we performed also simulations for the experimentally investigated mixtures. In order to study the influence of the rigidity of bonds, we included also 2,3-DMPEN and 2,4-DMPEN. Figure 5.4 shows a typical temperature and mole fraction

profiles for equimolar mixtures of heptane in *p*-xylene. These profiles were found to be linear, so that the temperature and the concentration gradients can be easily calculated. The average fluctuation of the concentration is 8%, and the temperature variation is 2 K in each slab.

Figure 5.5 shows the simulated Soret coefficient for different alkane (alkene)/aromatic compound mixtures. For all considered solvents, the magnitude of the Soret coefficient becomes smaller with increasing degree of branching of the first component. For the mixtures with xylenes, the shapes of the curves are not sensitive to the nature of the second component and the substitution of *o*-xylene by *p*-xylene makes the magnitude of S_T smaller, which confirms the experimental trend (cf. Figure 5.2), but the simulation data are systematically to low. Or in other words, their magnitude is too large, which means that the simulations predict a larger separation of the compounds compared to the experiment. In some cases such as 2,3-DMP/ heptane, the values differ by a factor of 2, but nevertheless, the branching effect is also clearly visible in the simulations. If we look at the influence of the rigidity of bonds on the Soret coefficient by comparing the results for alkedienes and alkanes, we notice there is a stronger tendency for the alkedienes to move to the warm side. Figure 5.5 shows some intersection points which were not observed in the experiment (cf. Figure 5.2). The possible reason could be an inconsistency of the force fields used. The Lennard-Jones parameters used for benzene and cyclohexane were different from the ones for *p*-xylene and *o*-xylene, as explained in section 5.3

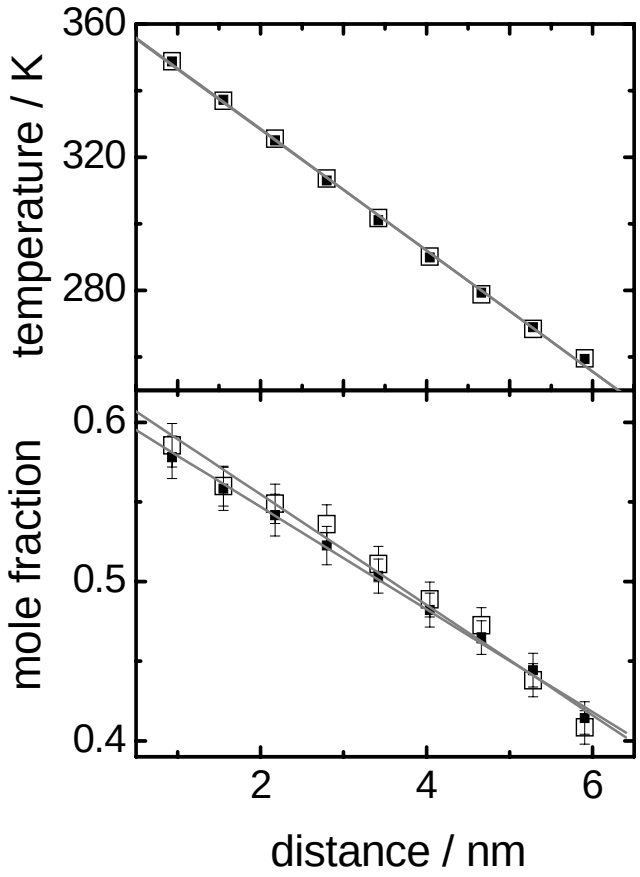

Figure 5.4: The temperature and mole fraction profiles for *n*-heptane/p-xylene mixture. The open and solid symbols refer to first 9 slabs and reversed in *x* direction last 9 slabs of the simulation box.

In the previous work[7] has been shown that the simple conception found for Lennard Jones mixtures is not capable to explain the effect of branching in heptane/benzene mixtures. This approach is also not able to explain the thermal diffusion behavior of alkane(alkene)/p-xylene and alkane(alkene)/o-xylene mixtures.

Although the validity of the Hildebrandt solubility parameter concept is not sufficient to describe the thermodiffusive motions,[25] there are several examples in the literature where a correlation has been found. For instance, the Soret coefficient of spherical molecules[4] shows a correlation with the energy density. Also, for a thermosensitive polymer[26] in different alcohols, the concentration at which the Soret

coeffcient changes sign is correlated with the Hildebrandt solubility parameter. Furthermore, the simulations of Lennard-Jones liquids show a correlation between the Soret coefficient and the potential energy density of a species.[2]

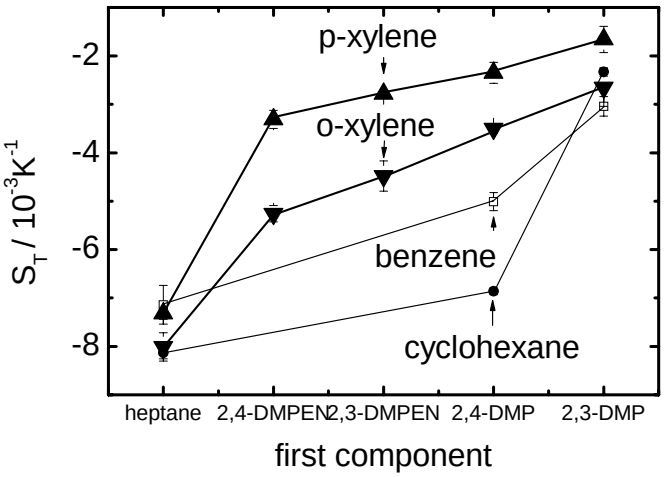

Figure 5.5: The simulated Soret coefficients for equimolar mixtures of some alkanes and alkenes in different solvents.

Figure 5.6 shows the calculated Soret coefficient for ten xylene mixtures versus the difference in Hildebrandt parameters ($\Delta\delta$) of the mixing partners, which is defined as square roots' subtraction of solvents' and solutes' cohesive energy density. The Hildebrandt parameter has been calculated from equilibrium molecular dynamic simulations using the so-called nonbonded energy.[2,10] The magnitude of S_T becomes smaller with increasing $\Delta\delta$ for heptane, 2,3-DMP and 2,4-DMP, what is not the case for the mixture of spherical LJ particles.[2] On the other hand, if one compares 2,3-DMPEN and 2,4-DMPEN with heptane, the opposite trend can be observed. One can expect that a larger $\Delta\delta$ increases the difference between the mixing partners, resulting in a larger value of the magnitude of S_T. It is obvious that we cannot confirm this simple correlation. Even for those nonpolar solvents, the thermal diffusion behavior is guided by a delicate balance of cross and pure interactions between the mixing partners.

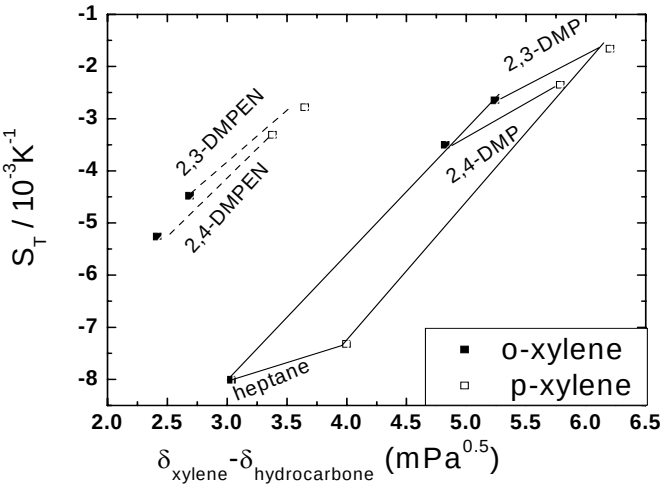

Figure 5.6: The simulated Soret coefficient (p-xylene: solid symbols, o-xylene: open symbols) plotted versus the difference in the Hildebrandt parameter of the mixing partners.

5.4. Conclusions

The Soret coefficients of equimolar mixtures of heptanes (heptane, 2,3-DMP, and 2,4-DMP) in cyclohexane, *p*-xylene, and *o*-xylene were determined using the TDFRS technique and the RNEMD method. In the simulation, we considered 2,3- DMPEN and 2,4-DMPEN, additionally. Both approaches show the decrease of the magnitude of *S*T with increasing degree of branching, but the value determined by simulation is systematically too small, while its magnitude is too large. We could assign to each component a *heat affinity*, which allows the calculation of the Soret coefficient of the mixture and could be related to the heat of evaporization, density, mass, and assymmetry of the pure component. The magnitude of the Soret coefficient does not increase with the difference in Hildebrandt parameters of the mixing partners, as is expected for the mixtures of Lennard- Jones particles.

In order to gain a better understanding, further investigations of the thermal diffusion on a microscopic level and a detailed molecular dynamic analysis of the orientation dynamics in equilibrium and nonequilibrium will be necessary. The goal will be to identify the important parameters and properties, which have the largest influence on the thermal diffusion behavior.

5.5. References

[1] S. Wiegand, J. Phys.-Condes. Matter **16** (10), R357 (2004).

[2] D. Reith and F. Müller-Plathe, J. Chem. Phys. **112** (5), 2436 (2000).

[3] G. Galliero, B. Duguay, J. P. Caltagirone, and F. Montel, Fluid Phase Equilib. **208** (1-2), 171 (2003).

[4] P. Polyakov, M. Zhang, F. Müller-Plathe, and S. Wiegand, J. Chem. Phys. **127** (1) (2007).

[5] H. Kramers and J. J. Broeder, Anal. Chim. Acta **2** (5-7), 687 (1948).

[6] A. L. Jones and E. C. Milberger, Indust. and Eng. Chem. **45** (12), 2689 (1953); K. Shukla and A. Firoozabadi, Ind. Eng. Chem. Res **37** (8), 3331 (1998); A. Leahy-Dios and A. Firoozabadi, Aiche J. **53** (11), 2932 (2007); P. Blanco, M. M. Bou-Ali, J. K. Platten, P. Urteaga, J. A. Madariaga, and C. Santamaria, J. Chem. Phys. **129** (17) (2008); A. Leahy-Dios, L. Zhuo, and A. Firoozabadi, J. Phys. Chem. B **112** (20), 6442 (2008).

[7] P. Polyakov, J. Luettmer-Strathmann, and S. Wiegand, J. Phys. Chem. B **110** (51), 26215 (2006).

[8] P. Polyakov, F. Müller-Plathe, and S. Wiegand, J. Phys. Chem. B **112** (47), 14999 (2008).

[9] F. Müller-Plathe, J. Chem. Phys. **106** (14), 6082 (1997).

[10] G. Milano and F. Müller-Plathe, J. Phys. Chem. B **108** (22), 7415 (2004).

[11] M. G. Martin and J. I. Siepmann, J. Phys. Chem. B **102** (14), 2569 (1998).

[12] C. D. Wick, M. G. Martin, and J. I. Siepmann, J. Phys. Chem. B **104** (33), 8008 (2000).

[13] J. P. Ryckaert, G. Ciccotti, and H. J. C. Berendsen, J. Comput. Phys. **23** (3), 327 (1977); F. Müller-Plathe and D. Brown, Comput. Phys. Commun. **64** (1), 7 (1991).

[14] F. Müller-Plathe, Comput. Phys. Commun. **78** (1-2), 77 (1993); K. B. Tarmyshov and F. Müller-Plathe, J. Chem Inf. Model. **45** (6), 1943 (2005).

[15] H. J. C. Berendsen, J. P. M. Postma, W. F. van Gunsteren, A. Dinola, and J. R. Haak, J. Chem. Phys. **81** (8), 3684 (1984).

[16] http://sciencelab.com, The density for para- and orto-xylenes has been found at the website.

[17] J. S. Chickos, S. Hosseini, and D. G. Hesse, Thermochim. Acta **249**, 41 (1995).

[18] Nafisimo.J, J. B. Birks, and K. R. Naqvi, Proc. Phys. Soc. of London **91** (572P), 449 (1967).

[19] G. Wittko, Ph.D. thesis, University Bayreuth, Germany (2007).

[20] R. Weast, CRC Handbook of Chemistry and Physics, vol. 58th ed **CRC Press Inc., New York,** (1977).

[21] J. S. Chickos and W. E. Acree, J. Phys. Chem. Ref. Data **32** (2), 519 (2003).

[22] Chem3d, ver. 10 (2006).

[23] C. Debuschewitz and W. Kohler, Phys. Rev. Lett. **87** (5) (2001).

[24] K. I. Morozov, Phys. Rev. E **79** (3) (2009).

[25] P. A. Artola, B. Rousseau, and G. Galliero, J. Am. Chem. Soc. **130** (33), 10963 (2008).

[26] R. Kita and S. Wiegand, Macromolecules **38** (11), 4554 (2005).

Chapter 6: Summary

The successful applications of melt polystyrene (PS) in the automotive, electrical and electronics, consumer and industrial areas offers a unique combination of heat resistance, chemical resistance, and good electrical properties.[1] Therefore, thermal properties studies of biaxially oriented crystal PS film is essential because it can open the door to another market where clarity and strength properties make it ideal for many new applications.[2] Pending a pure crystal has been not attained yet, the thermal conductivity of the crystalline polymer can be calculated only by simulation, as has been done in this work.

Non equilibrium MD simulations were employed for the calculation of thermal conductivity of the δ modification of syndiotactic polystyrene and so-called compact structure, which has a density similar to the crystalline α and β forms of s-PS, but not their crystal structure. To the best of our knowledge, it was the first time where the estimation of the value of polymer crystal thermal conductivity has been done by computer simulation and anisotropy has been evaluated. We tested six different force field sets, which were varied in the number of degrees of freedom. It was found that the thermal conductivity is sensitive to the number of degrees of freedom of the system. Fully atomistic models with all flexible bonds always overestimates experimental values, as was found in previous publication[3], whereas the fully constrained bonds in repeat unit in our model yield an average value of the conductivity in all directions that is in excellent agreement with experimental data. It is important to note that stiffness of bonds in the backbone has a higher influence on the thermal conductivity than stiffness of the bonds in the pendant groups of the polymer.

Due to the polymer's oriented structure, anisotropy of the thermal conductivity was observed, which can be applied in various fields of technology. The heat conduction parallel to the polymer chains is 2.5–3 times larger than perpendicular to it. Even in the values of the thermal conductivities of two perpendicular directions small differences were observed.

Our research is not limited to only studies of polymer's thermal conductivity. Singe polymers are also widely used for interfaces in the second project has been to analyze the data, which is essential for bulk definition in interfaces studies.

Polymer interfaces are of considerable technological importance for products ranging from reflectors for car lights, compact discs, and electrically shielded computer cases to foils for food packaging.[4] But polymer absorption on a surface significantly changes dynamic (like mean-squared displacement, diffusion, orientation correlation function) and static properties (like density, gyration radii, radii distribution function).[5] Then, to distinguish the interface between polymer and surface, the simulated system must contain the bulk region of polymer. Therefore, in Chapter 4 we discussed the morphology of small polyvinyl alcohol oligomers with different chain lengths (N=1,2,3,5,7,10). The linear dependence between specific volume of the polymers and inverse of the number of repeat units is found in the previous publication of Dollhopf *et al*. for *n*-alkanes.[6] The density at $N \to \infty$ was interpolated from the observed dependence for the polymer at 400K and at 300K and compared to experimental data. RDFs between different parts of oligomers have been illustrated. We have shown that intramolecular interactions are dominant for long chains. Gyration radii were calculated and are in good agreement with theoretical studies.

Unfortunately, often it is difficult to calculate dynamic properties for polymers because of slow diffusion. In spite of that, the orientation correlation function for different bonds in the chain was calculated and from it the relaxation time has been determined. The Kohlrausch-Williams-Watts expression was used to fit and integrate the orientation correlation functions (OCF) to obtain the relaxation times. The relaxation time for most of the bonds scales exponentially with the chain length up to N=5. The mean square displacement (MSD) of the hydroxyl oxygens and backbone carbon atoms in all PVA melts has been evaluated. A linear behavior of the MSDs as a function of time can be observed for short oligomers. For the long oligomers, the diffusion of the atoms within the first picoseconds is faster (so-called "free diffusion"). The oligomers discussed in these studies are not long enough for observation of the Rouse model.

And finally in the last topic of the thesis we came back to the thermal properties where the Soret coefficient of mixtures has been calculated. The aim of Chapter 5 is to gain a better understanding of the thermal diffusion behavior in liquid mixtures. First, we investigated liquid binary systems of spherical, chain-like and associated simple molecules by thermal diffusion. The influence of physical properties like mass, density, Hildebrandt parameter (see later the definition) etc. on S_T is analyzed. We calculated the Soret coefficient for mixtures of xylene with the different isomers of heptane (heptene). It is important to note that by theory all mixtures may have a similar Soret coefficient because the mass, size and interactions for each solvent/solute are the same. Differences are found in the structure and shape, which cause different moment of inertia. We expected that the planarity of alkene and xylene will result in a better "fitting" to each other which could lead to reduction in the thermal diffusion. In despite of that our expectations were erroneous. Previous publications reported a correlation between the Soret coefficient and the Hildebrandt parameter, [7] which is defined as $(\sqrt{\frac{H_v - RT}{V_m}})_{first\_component} - (\sqrt{\frac{H_v - RT}{V_m}})_{second\_component}$ where H_v is heat of vaporization and V_m is molar volume, but it was not confirmed in our results. Most of the simulation data has been compared to experimental values and good agreement has been found.

References

[1] J. Schellenberg and H. J. Leder, Adv. Polym. Technol. **25** (3), 141 (2006).

[2] P. L. Ku, Adv. Polym. Tech. **8**, 177 (1988).

[3] E. Lussetti, T. Terao, and F. Müller-Plathe, J. Phys. Chem. B **111** (39), 11516 (2007).

[4] K. L. Mittal, Metallized Plastics: Fundamentals and Applications, Marcel Dekker, New York 1998.

[5] C. F. Abrams, L. Delle Site, and K. Kremer, Phys. Rev. E **67** (2) (2003).

[6] W. Dollhopf, H. P. Grossmann, and U. Leute, Colloid Polym. Sci. **259** (2), 267 (1981).

[7] S. Wiegand, J. Phys.-Condes. Matter **16** (10), R357 (2004).

Publications

This thesis has led to the following publications

1. Rossinsky E., Müller-Plathe F. *J. Chem. Phys*., 130, 2009 "Anisotropy of the thermal conductivity in a crystalline polymer: Reverse nonequilibrium molecular dynamics simulation of the σ phase of syndiotactic polystyrene"
2. Rossinsky E., Tarmyshov K.B., Böhm M.B., Müller-Plathe F*., Macromol. Theory and Simulation*, 18, 2009 "Properties of polyvinyl alcohol oligomers: A molecular dynamics study"
3. Polyakov P., Rossinsky E., Wiegand S., *J. Phys. Chem. B*, 113**,** 2009, "Study of the Soret effect in hydrocarbon chains/aromatic compound mixtures"

Curriculum Vitae

Name: Eduard Rossinsky
Date of birth: 04.11.1977
Born in: Belgorod, Russian Federation
Citizenship: Israel

School education:

1985-1992 **primary and secondary school N9**, Belgorod, Russian Federation

1993-1995 **Gymnasium N1**, Belgorog, Russian Federation

Higher Education:

1996-2000 **Technion - Israel Institute of Technology**, Haifa, Israel
B.Sc.Chemical Engineering

2003-2006 **Technion - Israel Institute of Technology**, Haifa, Israel
M.Sc.Chemical Engineering

2006-2009 **Technische Universität Darmstadt**, Darmstadt, Germany
Computational Chemistry, PhD student

Work experience:

1997-1998 **Research Institute in Chemical Engineering ("TAMI"),** Israel
Responsible for process robustness of the pilot plant.

2000- 2003 **IDF (Israel Defence Force)**
Officer in Chemical Engineering

2003-2006 **Technion - Israel Institute of Technology**, Haifa, Israel
Teaching Asssistant

24.10.2009, Frankfurt

Eduard Rossinsky **Data**

Eduard Rossinsky
2009
Neckarstr 15
64283 Darmstadt
Germany

Darmstadt, den 26, Oktober,

Eidesstattliche Erklärung

Ich erkläre hiermit an Eides statt, dass ich meine Dissertation selbstständig und nur mit den angegebenen Hilfsmitteln angefertigt

_____
(Eduard Rossinsky)

Eduard Rossinsky
2009
Neckarstr 15
64283 Darmstadt
Germany

Darmstadt, den 26, Oktober,

Erklärung

Ich erkläre hiermit, noch keinen Promotionsversuch unternommen zu haben.

_____
(Eduard Rossinsky)